diameter area. The final platelet aggregation pressure of each reaction tube was determined as the pressure rate of a pressure sensor connected to the syringe. The pressure rate was standardized by a grading curve; 1, 2, 4 and 8 μmol/l ADP were plotted on the *x* axis and the pressure rates (%) were plotted on the *y* axis. Figure 1 shows a representative analysis of platelet aggregation by the WB aggregometer using a grading curve. The concentration of ADP inducing a 50% pressure rate was calculated and indicated as the platelet aggregatory threshold index (PATI). PATI values were used to evaluate WB aggregation.

Time course change in the PATI after blood collection and reproducibility in WB aggregation

To investigate changes in the PATI after blood collection over time, WB aggregation was measured at 5, 15, 30, 60 and 120 min after blood collection in eight healthy volunteers. The reproducibility of WB aggregation was also examined in blood samples. At 60 min after blood collection, the PATI values determined from WB on one day were compared with values from another day when the same measurements were performed.

Fig. 1

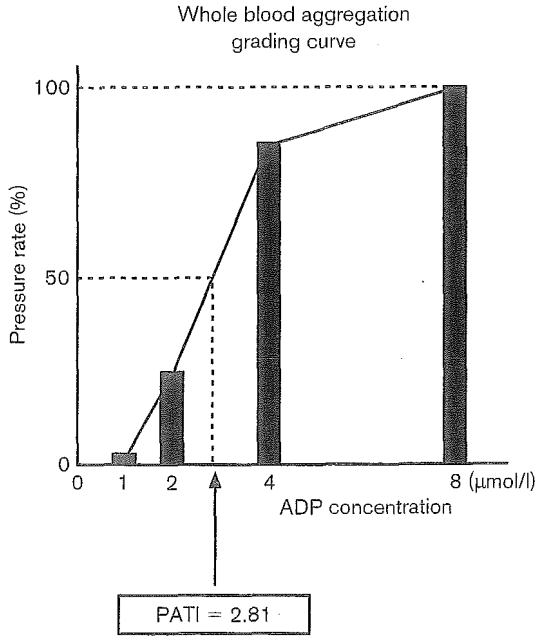

A representative analysis of whole blood aggregation using a grading curve. The *x* axis is adenosine diphosphate (ADP) concentration, and the *y* axis is pressure rate (%). The concentration of ADP inducing 50% pressure rate was calculated and indicated as a platelet aggregatory threshold index value. Whole blood aggregation was measured at 60 min after blood collection. PATI, platelet aggregatory threshold index.

Estimation of drug effects on WB aggregation and its comparison with PRP aggregation

At 60 min after blood collection, the working solutions of aspirin, cilostazol and ramatroban were added to WB, followed by incubation for 3 min. Drug-treated WB was stimulated by ADP and WB aggregation was measured as already described. In addition, PATI values in PRP aggregation were also calculated from light transmission 5 min after ADP addition in a similar manner to WB (Fig. 2), and were compared with those in WB aggregation.

Co-existence of platelets and leukocytes on the microsieve

To investigate the co-existence of platelets and leukocytes on the microsieve after WB aggregometry, staining of platelets and leukocytes was performed by use of dual-colour immunofluorescence. Erythrocytes on the microsieve were lysed with lysis buffer containing NH_4Cl, $NaHCO_3$ and EDTA2Na, and then were fixed with commercially available solution (Cell Fix; Becton Dickinson, San Jose, California, USA). After being washed three times, the microsieves were pre-incubated with 5% bovine serum albumin in phosphate-buffered saline (pH 7.4) at room temperature. After removing the solution, the microsieves were incubated with saturating concentrations of PE-conjugated anti-CD42b and FITC-conjugated anti-CD45 in a total volume of 500 μl phosphate-buffered saline containing 2% bovine serum albumin for 4 h at 4°C in the dark, then washed five times with phosphate-buffered saline. Images of the immunofluorescent samples were obtained using a CSU-10 confocal laser scanning unit (Yokogawa Electric Co., Tokyo, Japan) coupled to an IX90 inverted microscope with UPlanAPO × 20 objective lens (Olympus Optical Co., Tokyo, Japan) and a C5810-01 colour chilled 3CCD camera (Hamamatsu Photonics K. K., Hamamatsu, Japan) [30,31].

Statistical analysis

The data are expressed as means ± standard deviation. Statistical analysis was performed by a one-way analysis of variance, which was followed by Fisher's protected least significant difference test. Relationships between independent variables were assessed by Pearson's correlation. Differences were considered to be significant at $P < 0.05$. StatView J-4.5 software (Abacus Concepts Inc., Berkeley, California, USA) was employed for all calculations.

Results

Inhibitory effects of aspirin, cilostazol and ramatroban on PRP aggregation

MA values from control PRP in response to ADP (1 and 5 μmol/l), collagen (1 μg/ml) and arachidonic acid (3 mmol/l) are presented in Table 1. When control PRP was stimulated by 1 μmol/l ADP, primary aggregation was induced in all specimens, with MAs of 40% or less,

Fig. 2

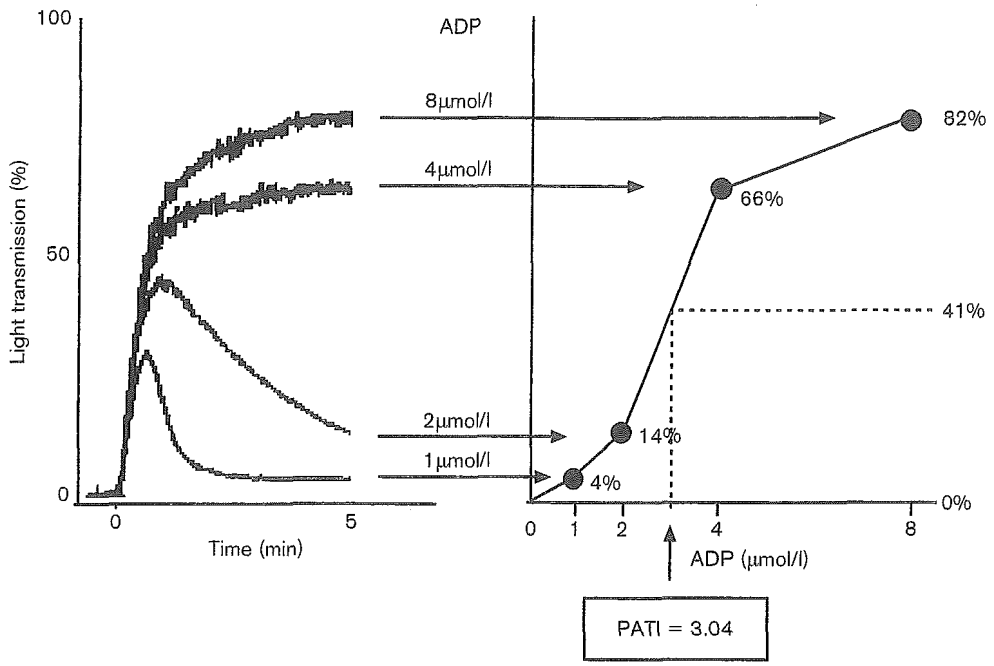

Representation of platelet-rich plasma (PRP) aggregation using the platelet aggregatory threshold index (PATI) value. Left panel shows a representative PRP aggregation by the turbidimetric method. When light transmission 5 min after adenosine diphosphate (ADP) addition is plotted on the grading curve (right panel) and the maximum light transmission value (82%) with 8 μmol/l ADP-induced aggregation is regarded as 100%, the PATI value is calculated as the concentration of ADP causing a 50% light transmission (i.e. 41%) on the grading curve.

Table 1 Circulating plasma levels of sP-selectin, transforming growth factor-beta 1 (TGF-β1) and thromboxane B_2 (TXB_2) and platelet responses in control platelet-rich plasma after stimulation by agonists

		Agonists			
	Circulating plasma levels	ADP 1 μmol/l	ADP 5 μmol/l	Collagen 1 μg/ml	Arachidonic acid 3 mmol/l
MA (%)		36 ± 4	82 ± 2*	84 ± 4*	85 ± 4*
sP-selectin (ng/ml)	98 ± 16	129 ± 9	228 ± 22*	288 ± 29*	239 ± 32*
TGF-β1 (ng/ml)	2.5 ± 0.8	8.8 ± 2.3	28.5 ± 4.2*	38.3 ± 5.6*	47.9 ± 7.0*
TXB_2 (ng/ml)	1.2 ± 0.4	5.5 ± 2.6	54.7 ± 16.7*	249.8 ± 34.0*	478.4 ± 90.8*

Data represent mean ± standard deviation ($n = 8$). MA, percentage maximum aggregation; sP-selectin, soluble P-selectin. *$P < 0.01$ versus the value in response to 1 μmol/l adenosine diphosphate (ADP) (Fisher's protected least significant difference test).

while strong aggregation with MAs of 78% or more was seen in response to 5 μmol/l ADP, collagen and arachidonic acid.

The inhibitory effects of aspirin, cilostazol and ramatroban on PRP aggregation induced by ADP (5 μmol/l), collagen and arachidonic acid were examined. Inhibitory effects of these drugs increased in a concentration-dependent manner (data not shown). As shown in Figure 3a, the percentage decreases in MA values of aspirin at 100 μmol/l, cilostazol at 10 μmol/l and ramatroban at 1 μmol/l after stimulation by ADP were 34, 34 and 33%, respectively. As shown in Figure 3b, the percentage changes in MA after stimulation by collagen were 77% with 100 μmol/l aspirin, 35% with 10 μmol/l cilostazol and 65% with 1 μmol/l ramatroban, respectively. Percentage decrease in MA of 100 μmol/l aspirin, 10 μmol/l cilostazol and 1 μmol/l ramatroban, in response to arachidonic acid, were 83, 38 and 71%, respectively (Fig. 3c).

Inhibitory effects of aspirin, cilostazol and ramatroban on the release of intraplatelet substances

The levels of sP-selectin, TGF-β1 and TXA_2 from control PRP in response to ADP, collagen and arachidonic acid are presented in Table 1. When control PRP

Fig. 3

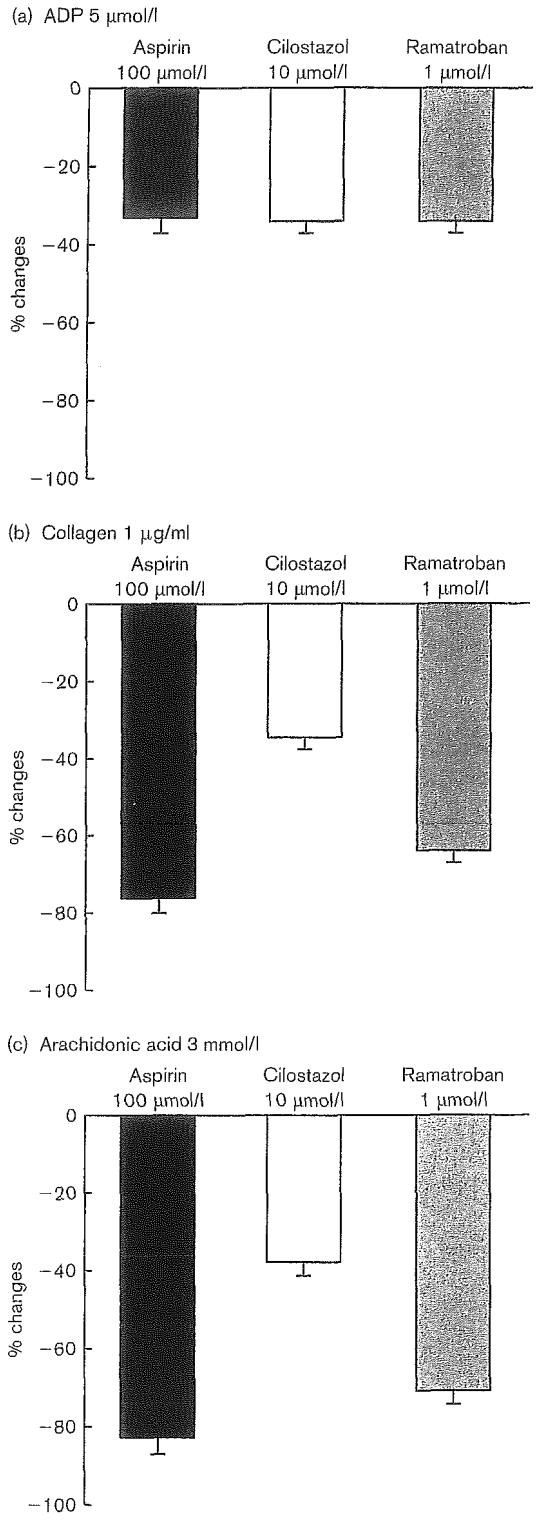

Inhibitory effects of aspirin, cilostazol and ramatroban on platelet-rich plasma (PRP) aggregation induced by (a) adenosine diphosphate (ADP) (5 μmol/l), (b) collagen (1 μg/ml) and (c) arachidonic acid (3 mmol/l). PRP samples were pre-incubated with drugs for 3 min prior to the addition of agonists. Effects of drugs were evaluated as percentage changes in maximum aggregation against vehicle-treated samples. Data represent mean ± standard deviation ($n = 8$).

was stimulated by 1 μmol/l ADP, sP-selectin and TGF-β1 levels increased significantly compared with their circulating plasma levels ($P < 0.05$). TXB_2 also showed high levels, although no difference was found between the levels in response to 1 μmol/l ADP and the levels in circulating plasma. The levels of sP-selectin, TGF-β1 and TXB_2 in response to 5 μmol/l ADP, collagen (1 μg/ml) and arachidonic acid (3 mmol/l) were significantly higher than those in response to 1 μmol/l ADP ($P < 0.001$). Furthermore, TXB_2 levels in response to arachidonic acid markedly increased compared with those in response to 5 μmol/l ADP ($P < 0.001$).

The inhibitory effects of aspirin, cilostazol and ramatroban on the release of P-selectin, TGF-β1 and TXA_2 from platelets in response to ADP (5 μmol/l), collagen and arachidonic acid are shown in Figure 4. When PRP was stimulated by ADP (5 μmol/l), 100 μmol/l aspirin significantly inhibited the release of TXA_2 compared with that of P-selectin and TGF-β1. In contrast, inhibitory effects of 10 μmol/l cilostazol and 1 μmol/l ramatroban on the release of TXA_2 in response to ADP (5 μmol/l) were similar to those on the release of P-selectin and TGF-β1. Aspirin and ramatroban markedly inhibited the release of P-selectin, TGF-β1 and TXA_2 to a similar degree in response to collagen and arachidonic acid. However, 10 μmol/l cilostazol inhibited the release of the three molecules in response to ADP, collagen and arachidonic acid to a similar degree.

Time-dependent change after blood collection and reproducibility in WB aggregation

In order to investigate the relationship between ADP concentration and pressure rate, WB aggregation induced by 1, 2, 4 and 8 μmol/l ADP was measured. As shown in Figure 5a, when control WB and aspirin-treated (10, 50, 100 and 500 μmol/l) WB were stimulated by ADP, the pressure rates in all samples increased depending on ADP concentrations. These data were presented as the dose–response plots for aspirin concentrations in Figure 5b. PATI values elevated with the increase in aspirin concentration. Figure 6 shows time-dependent changes in the PATI values after blood collection. PATI values immediately after blood collection (5 min) were 5.68 ± 1.71, and decreased gradually until 60 min after blood collection, and then increased slightly after 120 min. The following experiments to evaluate WB aggregation were performed using blood samples 60 min after collection. In the examination of reproducibility between two different sample days, the mean values of PATI from the same volunteers were 2.63 ± 0.65 and 2.52 ± 0.84 ($n = 8$), respectively, and no significant difference in PATI values between the two days was observed. While platelet counts from eight volunteers ranged from 17.5×10^4 to 31.2×10^4 cells/μl [mean platelet count, $(25.0 \pm 5.0) \times 10^4$ cells/μl], PATI values were in

Fig. 4

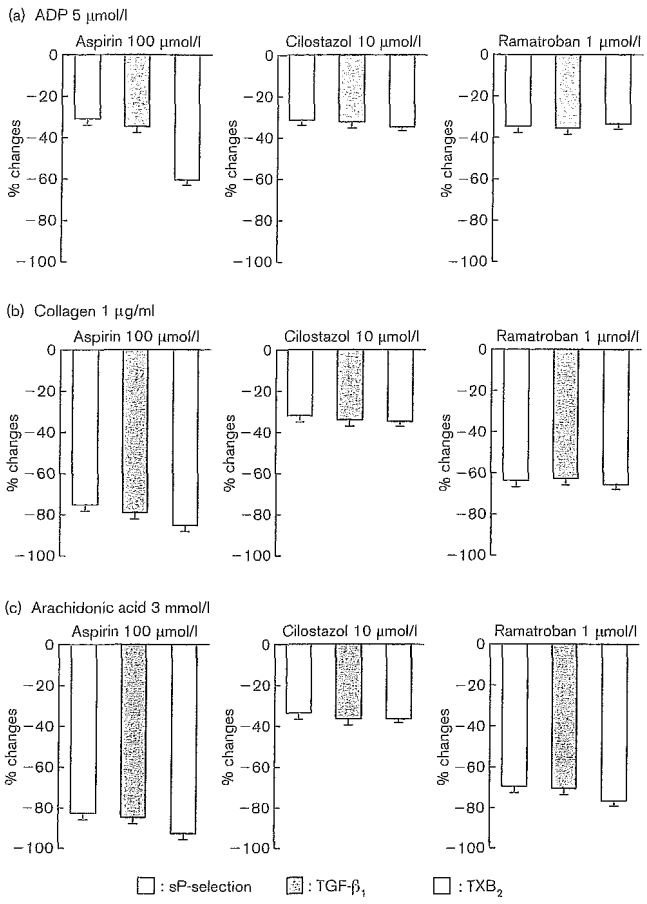

Inhibitory effects of aspirin, cilostazol and ramatroban on release reaction in response to (a) adenosine diphosphate (ADP), (b) collagen and (c) arachidonic acid. Platelet-rich plasma (PRP) samples were pre-incubated with drugs for 3 min prior to the addition of ADP (5 μmol/l), collagen (1 μg/ml) and arachidonic acid (3 mmol/l). Levels of soluble P-selectin (sP-selectin), transforming growth factor-beta 1 (TGF-β1) and thromboxane B_2 (TXB_2) were measured as described in Materials and methods. Effects of drugs on each parameter were evaluated as percentage changes against vehicle-treated samples. Data represent mean ± standard deviation ($n = 8$).

the range of 2.28–3.87 μmol/l (mean, 2.98 ± 0.52 μmol/l). There was no correlation between platelet counts and PATI values.

Inhibitory effects of aspirin, cilostazol and ramatroban on WB and PRP aggregation induced by ADP (1, 2, 4 and 8 μmol/l)

When aspirin-treated, cilostazol-treated and ramatroban-treated WB were stimulated by ADP (1, 2, 4 and 8 μmol/l), the PATI values increased depending upon concentration of the respective drugs, reaching 7.15 ± 0.70 with 500 μmol/l aspirin, 7.33 ± 0.86 with 50 μmol/l cilostazol and 7.91 ± 0.18 with 10 μmol/l ramatroban. Next, these changes in PATI values on WB aggregation were compared with those on PRP aggregation induced by same concentration of ADP. The PATI values from drug-treated PRP also elevated in a concentration-dependent manner, reaching 5.50 ± 1.86 with 500 μmol/l aspirin, 7.36 ± 0.89 with 50 μmol/l cilostazol and 4.53 ± 0.50 with 10 μmol/l ramatroban. Inhibitory effects of aspirin, cilostazol and ramatroban on both WB and PRP aggregation were expressed as the percent increase of PATI values against control samples. As shown in Figure 7, increases of PATI by aspirin and cilostazol on both WB and PRP aggregation were found to be non-linear. In contrast, ramatroban resulted in the increase of PATI in a linear fashion. Cilostazol showed a steep increase of PATI in PRP compared with that in WB.

Confocal scanning laser microscopy

Figure 8 shows representative confocal and fluorescent images of platelets and leukocytes on the microsieve. When WB was stimulated by ADP (8 μmol/l), aggregates were observed on the microsieve in the confocal mode (Fig. 8a). In the same visual field as Figure 8a, platelets stained with PE-conjugated anti-CD42b showed red fluorescence (Fig. 8b), and leukocytes stained with FITC-conjugated anti-CD45 showed green fluorescence (Fig. 8c). Figure 8d indicates the co-existence of platelets and leukocytes.

Correlations between independent variables

The pressure rates of WB aggregation in aspirin-treated WB samples in response to ADP (1, 2, 4 and 8 μmol/l) were compared with the maximum aggregation rates of PRP aggregation and the released levels of sP-selectin, TGF-β1 and TXA_2 in aspirin-treated PRP samples stimulated by ADP (1, 2, 4 and 8 μmol/l). Correlation analysis was carried out between independent variables in aspirin-treated, cilostazol-treated, or ramatroban-treated WB and PRP samples in response to ADP (1, 2, 4 and 8 μmol/l). Close correlations were found between the pressure rate in WB aggregometry and other variables from PRP aggregometry, and between the PATI values from WB and PRP aggregation (Table 2).

Discussion

In the present study, we first examined the effects of aspirin, cilostazol and ramatroban on PRP aggregation induced by ADP (5 μmol/l), collagen (1 μg/ml) and arachidonic acid (3 mmol/l). The drugs inhibited PRP aggregation induced by ADP (5 μmol/l) in a concentration-dependent manner, and the effects of aspirin with 100 μmol/l, cilostazol with 10 μmol/l and ramatroban with 1 μmol/l were similar, showing an approximate 35% decrease in MA. Inhibitory effects of aspirin and ramatroban at these concentrations on collagen-induced and arachidonic acid-induced aggregation were stronger than those on ADP-induced aggregation. In contrast, inhibitory effects of 10 μmol/l cilostazol were similar in responsiveness when induced by the three agonists. The effects of ADP on platelets are mediated by at

Fig. 5

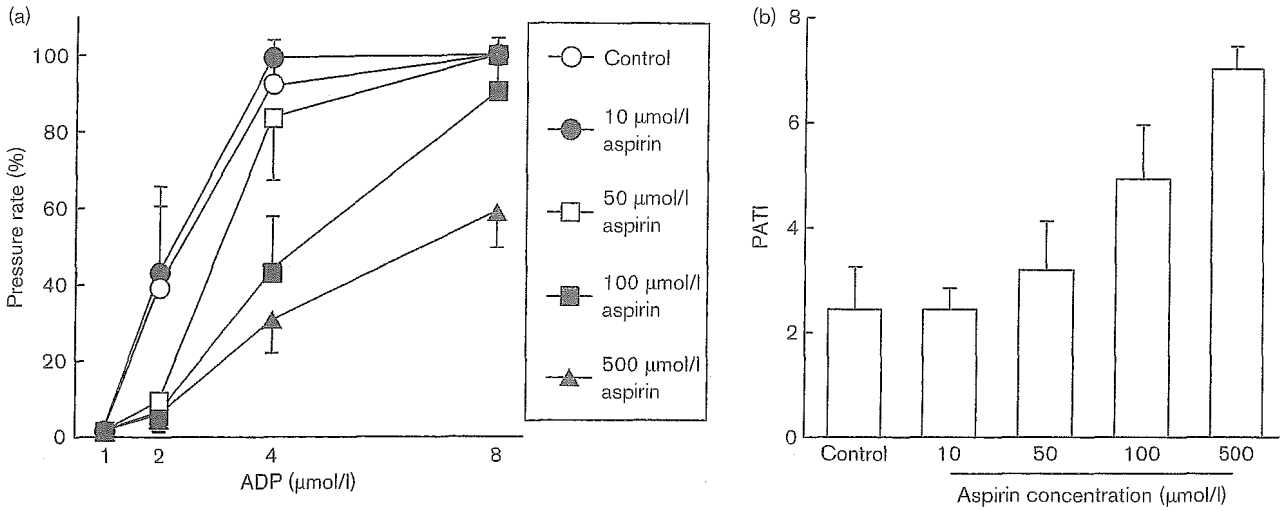

Relationship between adenosine diphosphate (ADP) concentration and pressure rate (%) in whole blood aggregation. Whole blood was pre-incubated with or without aspirin for 3 min prior to the addition of ADP (1, 2, 4 and 8 μmol/l). Whole blood aggregation was measured at 60 min after blood collection. Data represent mean ± standard deviation ($n = 8$). PATI, platelet aggregatory threshold index.

Fig. 6

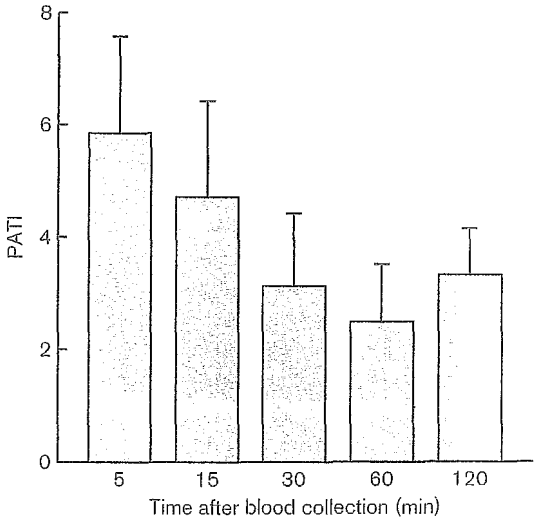

Time-dependent changes in platelet aggregatory threshold index (PATI) values after blood collection. Whole blood was stimulated by adenosine diphosphate (ADP) (1, 2, 4 and 8 μmol/l), and whole blood aggregation was measured at 5, 15, 30, 60 and 120 min after blood collection and PATI values were obtained. Data represent mean ± standard deviation ($n = 8$).

least three receptors; the P2X receptor that mediates rapid Ca ion influx, the P2Y1 receptor coupled to Gq-protein that stimulates phospholipase C (PLC) and induces shape change, and the P2TAC receptor coupled to the Gi-protein that inhibits adenylyl cyclase [32]. Since aspirin inhibited ADP-induced PRP aggregation to a certain degree in the present study, aspirin, a cyclooxygenase inhibitor, may cause the inhibition of PRP aggregation in response to ADP through the P2Y1 receptor. The effects of aspirin on platelet aggregation in response to collagen may be due to the inhibition of platelet activation via glycoprotein (GP) Ia/IIa (the $\alpha_2\beta_1$ integrin), CD36 (GPIV, also known as GPIIIb), or GPVI, which are collagen receptors and lead to PLCγ2 tyrosine phosphorylation and bring about TXA_2 formation [33]. GPIV may accelerate the rate of adhesion once platelets establish contact with collagen fibres via GPVI and GPIa/IIa [34]. Aspirin markedly inhibits PRP aggregation in response to arachidonic acid, because arachidonic acid is utilized in TXA_2 formation.

Next, we measured the levels of sP-selectin, TGF-β1 and TXB_2 in response to ADP, collagen and arachidonic acid. Aspirin markedly decreased TXB_2 levels compared with levels of sP-selectin and TGF-β1 in response to ADP. In contrast, the rates of decrease of TXB_2 by cilostazol and ramatroban were similar to those of sP-selectin and TGF-β1 in response to ADP. Furthermore, aspirin and ramatroban strongly inhibited the release of P-selectin, TGF-β1 and TXB_2 in response to collagen and arachidonic acid compared with the response induced by ADP. These results suggest that aspirin may inhibit not only TXA_2 formation via cyclooxygenase, but also could inhibit the release reaction of TXA_2 via activation of PLC. Stimulation of platelets by collagen and arachidonic acid induces TXA_2 production and the release reaction of intraplatelet substances. Ramatroban inhibits TXA_2 binding to the TXA_2 receptor on the surface of plate-

Fig. 7

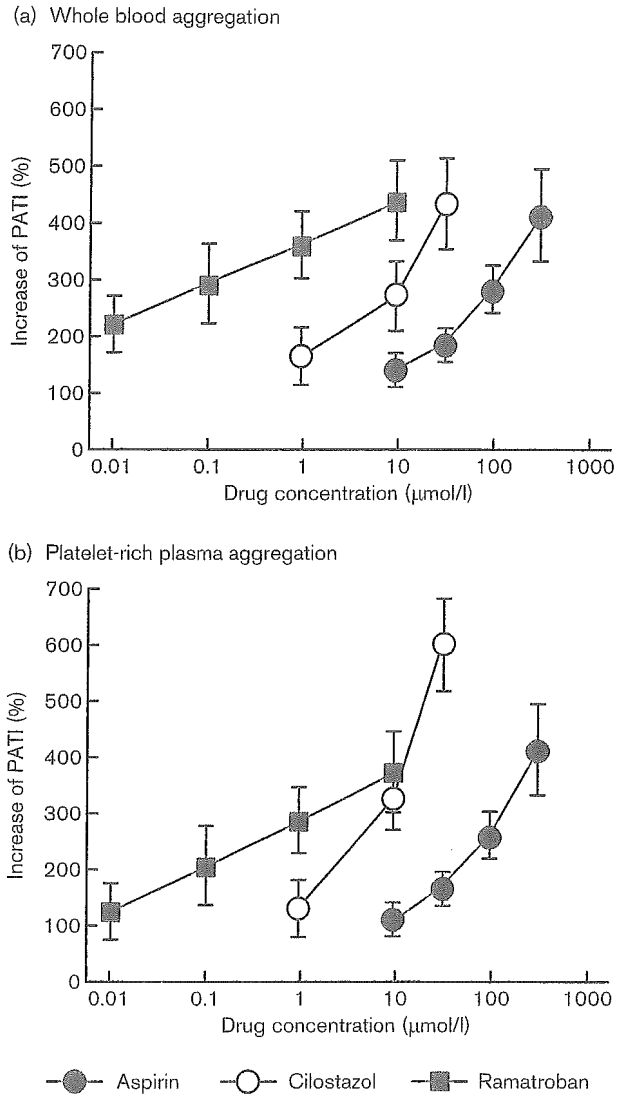

Inhibitory effects of aspirin, cilostazol and ramatroban on (a) whole blood and (b) platelet-rich plasma (PRP) aggregation. Whole blood and PRP samples were pre-incubated with aspirin, cilostazol and ramatroban for 3 min prior to the addition of adenosine diphosphate (ADP) (1, 2, 4 and 8 μmol/l). Percentage changes of platelet aggregatory threshold index (PATI) values for drug-treated samples against those for vehicle-treated samples were plotted along the vertical axis. Data represent mean ± standard deviation ($n = 8$). PATI values from vehicle-treated whole blood aggregation were 1.73 ± 0.30 for ethanol (aspirin and ramatroban) and 2.11 ± 0.70 for *N,N*-dimethylformamide (DMF) (cilostazol). PATI values from vehicle-treated PRP aggregation were 1.31 ± 0.30 for ethanol (aspirin and ramatroban) and 1.25 ± 0.23 for DMF (cilostazol).

lets. Therefore, while both aspirin and ramatroban inhibit the release of P-selectin, TGF-β1 and TXB_2 in response to collagen and arachidonic acid, released levels of TXB_2 in response to ADP are more strongly inhibited by aspirin than ramatroban. Evidence of this may be seen in the report that TXB_2 mediates platelet

Fig. 8

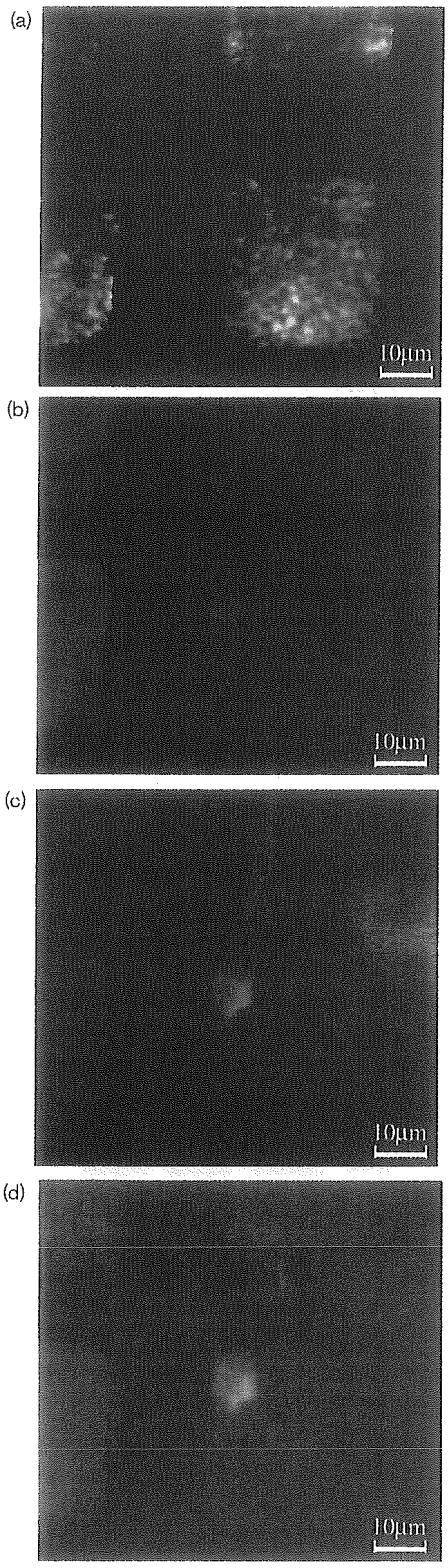

Confocal and fluorescent images of platelets and leukocytes on the microsieve. (a) When whole blood was stimulated by adenosine diphosphate (8 μmol/l), aggregates were observed on the microsieve in the confocal mode. (b), (c) and (d) Images of the fluorescent mode corresponding to the confocal mode.

Table 2 **Correlations between pressure rate in whole blood aggregometry and other independent variables from platelet-rich plasma (PRP) aggregometry**

	Whole blood:PRP	Coefficients (*R*)	*P* value
Aspirin-treated samples	Pressure rate:MA	0.849	< 0.001
	Pressure rate:sP-selectin	0.897	< 0.001
	Pressure rate:TGF-β1	0.920	< 0.001
	Pressure rate:TXB_2	0.737	< 0.001
	PATI:PATI	0.920	< 0.001
Cilostazol-treated samples	Pressure rate:MA	0.761	< 0.001
	Pressure rate:sP-selectin	0.823	< 0.001
	Pressure rate:TGF-β1	0.766	< 0.001
	Pressure rate:TXB_2	0.785	< 0.001
	PATI:PATI	0.828	< 0.001
Ramatroban-treated samples	Pressure rate:MA	0.638	< 0.001
	Pressure rate:sP-selectin	0.768	< 0.001
	Pressure rate:TGF-β1	0.774	< 0.001
	Pressure rate:TXB_2	0.802	< 0.001
	PATI:PATI	0.894	< 0.001

MA, percentage maximum aggregation; sP-selectin, soluble P-selectin; TGF-β1, transforming growth-factor-beta 1; TXB_2, thromboxane B_2; PATI, platelet aggregatory threshold index.

activation through a system linked to PLC [35]. Cilostazol inhibited the release of all the molecules in response to ADP, collagen and arachidonic acid in a similar fashion. These results may be due to the difference in pharmacological mechanisms between aspirin (a cyclooxygenase inhibitor), cilostazol (a phosphodiesterase III inhibitor) and ramatroban (a specific TXA_2 receptor antagonist). Different signal pathways in platelets most surely play important roles in these events.

Third, we examined the effects of these drugs on WB aggregation induced by ADP (1, 2, 4 and 8 μmol/l) using the newly developed WB aggregometer with the screen filtration pressure method, and the results were compared with those from PRP aggregation induced by the same agonist. To measure WB aggregation, some devices such as the PFA-100 [3,8], and the Ultegra Platelet Analyzer [3,9,10] have been developed. In the present study, a WB aggregometer with a microsieve made of nickel, 3.7 mm in diameter, with 300 openings/1 mm diameter area was used [15]. The pressure rate (%) of WB through the microsieve after stimulation by ADP (1, 2, 4 and 8 μmol/l) was measured. Although we did not compare data from this device with another WB aggregometer, it is reported that platelet aggregation data from the PFA-100 and the Ultegra correlated well to data from a four-channel Chrono-log Lumi-Aggregometer using PRP [10]. We obtained the result that the pressure rate (%) of WB through the microsieves and maximum aggregation rate (%) of PRP correlated closely. In addition, there were close correlations between PATI values from WB aggregation and PRP aggregation, and also between the pressure rate (%) of WB and the levels of molecules released from platelets. Therefore, we believe that data from the newly developed WB aggregometer bear a striking resemblance to other devices such as the PFA-100 and the Ultegra. Recently, the effects of anti-platelet drugs were successfully evaluated using the WB aggregometer with the screen filtration pressure method [16]. In the present study, we confirmed a high reproducibility of WB aggregation by this apparatus. On the other hand, the PATI value (which represents the concentration of ADP inducing a 50% pressure rate) was highest at 5 min after blood collection and then gradually decreased up to 60 min time, in accordance with previous reports [15,16]. Thus, the data from the WB aggregometer were variable over the time period studied. Although the reason why the PATI value varies depending on time has not yet been clarified, it is possible that a change in the responsiveness of receptors on blood cells or unstable anti-thrombotic physiological substances such as prostacyclin may be contributing factors [15]. Therefore, in clinical laboratories, it is necessary to decide on the time after blood collection determining WB aggregability in order to obtain accurate results. In addition, it is possible to use this device as a rapid bedside test by measuring immediately after blood collection.

In fact, clinical research on subjects who had taken aspirin for angina pectoris is now being conducted. Addition of ADP to WB samples collected from the patients was performed punctually 60 min after drawing blood. In our unpublished data, PATI values in WB aggregation on the seventh day after cessation of taking aspirin to prevent extra bleeding during surgery of coronary artery bypass grafting were lower than those in the aspirin-taking period (2.19 ± 1.33 versus 4.81 ± 2.03). These results suggest that the WB analyser with screen filtration pressure method is a useful instrument even in clinical aspects to evaluate the anti-platelet effects of drugs, as well as other devices.

We examined the in-vitro effects of drugs by comparing PATI values obtained from drug-treated WB at 60 min after blood collection. Aspirin and cilostazol inhibited WB aggregation in a concentration-dependent manner but in a non-linear fashion, while ramatroban inhibited linearly with increasing concentration. The difference in the increased pattern of the PATI values may be due to differences in pharmacological mechanisms between the three drugs. In our unpublished data, sarpogrelate hydrochloride, a 5-HT_2-serotonergic receptor antagonist, inhibited WB aggregation induced by simultaneous use of low concentration of collagen and serotonin linearly with increasing concentration from 0.1 to 100 μmol/l, showing a 200–500% increase of PATI values. It is of interest that enzyme inhibitors such as aspirin and cilostazol showed non-linear inhibition on WB aggregation, while receptor antagonists such as ramatroban and sarpogrelate suppressed in a linear fashion. The increase of PATI in PRP aggregation induced by ADP (1, 2, 4 and 8 μmol/l) showed a similar pattern to WB aggregation (Fig. 7). However, increases of PATI of 100 μmol/l aspirin and 10 μmol/l cilostazol on WB aggregation in response to ADP showed 292 and 272% increases, respectively, and were lower than that of 1 μmol/l ramatroban (388%) (Fig. 7a), and are different from the results of PRP aggregation induced by 5 μmol/l ADP (Fig. 3a).

We obtained confocal images that latticework openings on the microsieve after WB aggregation induced by ADP were filled with aggregates. Confocal fluorescence laser microscopy confirmed that the aggregates contained platelets and leukocytes. Thus, WB aggregometry using the screen filtration pressure method most probably reflects not only platelet–platelet aggregates, but also platelet–leukocyte conjugates.

In conclusion, we have more clearly clarified the difference in anti-platelet effects of drugs by investigating both PRP aggregation and release reaction in response to various agonists. It was demonstrated that the measurement of WB aggregation is also useful to evaluate the effects of drugs on platelet aggregation.

References

1 Ross R. Mechanisms of disease: atherosclerosis – an inflammatory disease. *N Engl J Med* 1999; **340**:115–126.
2 Hollenberg NK, Monterio K, Sandoz T. Endothelial injury provokes collateral arterial spasm: role of thromboxane and serotonin. *J Pharmacol Exp Therap* 1988; **244**:1164–1168.
3 Rand ML, Leung R, Packham MA. Platelet function assays. *Transfusion Apheresis Sci* 2003; **28**:307–317.
4 Ozaki Y, Satoh K, Yatomi Y, Yamamoto T, Shirasawa Y, Kume S. Detection of platelet aggregates with a particle counting method using light scattering. *Anal Biochem* 1994; **218**:284–294.
5 Yang L, Yatomi Y, Satoh K, Ozaki Y. Inhibitory effects of beraprost on platelet aggregation: comparative study utilizing two methods of aggregometry. *Thromb Res* 1999; **94**:25–32.
6 Cardinal DC, Flower RJ. The electronic aggregometer: a novel device for assessing platelet behavior in blood. *J Pharmacol Methods* 1980; **3**:147–154.
7 Ingerman-Wojenski C, Smith JB, Silver MJ. Evaluation of electrical aggregometry: comparison with optical aggregometry, secretion of ATP, and accumulation of radiolabeled platelets. *J Lab Clin Med* 1983; **101**:44–52.
8 Fattorutto M, Pradier O, Schmartz D, Ickx B, Barvais L. Does the platelet function analyser (PFA-100®) predict blood loss after cardiopulmonary bypass? *Br J Anaesth* 2003; **90**:692–693.
9 Smith JW, Steinhubl SR, Lincoff AM, Coleman JC, Lee TT, Hillman RS, *et al.* Rapid platelet-function assay: an automated and quantitative cartridge-based method. *Circulation* 1999; **99**:620–625.
10 Malinin AI, Atar A, Callahan KP, McKenzie ME, Serebruany VL. Effects of a single dose aspirin on platelets in humans with multiple risk factors for coronary artery disease. *Eur J Pharmacol* 2003; **462**:139–143.
11 Swank RL. Alteration of blood on storage: measurement of adhesiveness of 'aging' platelets and leukocytes and their removal by filtration. *N Engl J Med* 1961; **265**:728–733.
12 Dhall DP, Matheson NA. Platelet aggregate filtration pressure – a method of measuring platelet aggregation in whole blood. *Cardiovasc Res* 1969; **3**:155–160.
13 Faraday N, Scharpf RB, Dodd-o JM, Martinez EA, Rosenfeld BA, Dorman T. Leukocytes can enhance platelet-mediated aggregation and thromboxane release via interaction of P-selectin glycoprotein ligand 1 with P-selectin. *Anesthesiology* 2001; **94**:145–151.
14 Santos MT, Valles J, Marcus AJ, Safier LB, Broekman MJ, Islam N, *et al.* Enhancement of platelet reactivity and modulation of eicosanoid production by intact erythrocytes. *J Clin Invest* 1991; **87**:571–580.
15 Ozeki Y, Sudo T, Toga K, Nagamura Y, Ito H, Ogawa T, *et al.* Characterization of whole blood aggregation with a new type of aggregometer by a screen filtration pressure method. *Thromb Res* 2001; **101**:65–72.
16 Sudo T, Ito H, Ozeki Y, Kimura M. Estimation of anti-platelet drugs on human platelet aggregation with a novel whole blood aggregometer by a screen filtration method. *Br J Pharmacol* 2001; **133**:1396–1404.
17 Sudo T, Ito H, Kimura M. Characterization of platelet aggregation in whole blood of laboratory animals by a screen filtration pressure method. *Platelets* 2003; **14**:239–246.
18 Nakamura K, Kariyazono H, Moriyama Y, Toyohira H, Kubo H, Yotsumoto G, *et al.* Effects of sarpogrelate hydrochloride on platelet aggregation, and its relation to the release of serotonin and P-selectin. *Blood Coagul Fibrinolysis* 1999; **10**:513–519.
19 Kariyazono H, Nakamura K, Shinkawa T, Yamaguchi T, Sakata R, Yamada K. Inhibition of platelet aggregation and the release of P-selectin from platelets by cilostazol. *Thromb Res* 2001; **101**:445–453.
20 Moriyama Y, Nakamura K, Kariyazono H, Toyohira H, Taira A. Influence of low-intensity anticoagulation and low-dose antiplatelet agent on coagulation-fiblinolysis system after mechanical prosthetic valve replacement. *J Thorac Cardiovas Surg* 1998; **115**:952–954.
21 Nakamura K, Kariyazono H, Masuda H, Sakata R, Yamada K. Effects of sarpogrelate hydrochloride on adenosine diphosphate- or collagen-induced platelet responses in arteriosclerosis obliterans. *Blood Coagul Fibrinolysis* 2001; **12**:391–397.
22 Raines EW, Dower SK, Ross R. Interleukin-1 mitogenic activity of fibroblasts and smooth muscle cell is due to PDGF-AA. *Science* 1989; **243**:393–396.
23 Okazaki H, Majesky MW, Harker LA, Schwartz SM. Regulation of platelet-derived growth factor ligand and gene expression by α-thrombin in vascular smooth muscle cell. *Circ Res* 1992; **71**:1285–1293.
24 Grainger DJ, Wakefield L, Bethell HW, Farndale RW, Metcalfe JC. Release and activation of platelet latent TGF-β in blood clots during dissolution with plasmin. *Nat Med* 1995; 1:932–937.
25 Johnston GI, Cook RG, McEver RP. Cloning of GMP-140, a granule membrane protein, of platelets and endothelium: sequence similarity to proteins involved in cell adhesion and inflammation. *Cell* 1989; **56**:1033–1044.
26 McEver RP, Martin BR. A monoclonal antibody to a membrane glycoprotein binds only to activated platelets. *J Biol Chem* 1984; **259**: 9799–9804.
27 Nakamura K, Kariyazono H, Shinkawa T, Yamaguchi T, Yamashita T, Ayukawa O, *et al.* Inhibitory effects of H_2-receptor antagonists on platelet function *in vitro*. *Hum Exp Toxicol* 1999; **18**:487–492.
28 Kariyazono H, Nakamura K, Shinkawa T, Moriyama Y, Toyohira H, Taira A, *et al.* Inhibitory effects of antibiotics on platelet aggregation in vitro. *Hum Exp Toxicol* 1997; **16**:662–666.
29 Born GVR. Aggregation of blood platelets by adenosine diphosphate and its reversal. *Nature* 1962; **194**:927–929.
30 Motoori S, Majima HJ, Ebara M, Kato H, Hirai F, Kakinuma S, *et al.*

Overexpression of mitochondrial manganese superoxide dismutase protects against radiation-induced cell death in the human hepatocellular carcinoma cell line HLE. *Cancer Res* 2001; **61**:5382–5388.

31 Majima HJ, Nakanishi-Ueda T, Ozawa T. 4-Hydroxy-2-nonenal (5-NHE) staining by Anti-HNE antibody. In: Armstrong D (editor): *Oxidants and antioxidants: ultrastructure and molecular biology protocols*. Totowa, New Jersey: Humana Press, 2002; pp. 31–34.

32 Geiger J, Honig-Liedl P, Schanzenbacher P, Walter U. Ligand specificity and ticlopidine effects distinguish three human platelet ADP receptors. *Eur J Pharmacol* 1998; **351**:235–246.

33 Asselin J, Gibbins JM, Achison M, Lee YH, Morton LF, Farndale RW, *et al.* A collagen-like peptide stimulates tyrosine phosphorylation of syk and phospholipase Cγ2 in platelets independent of the integrin $\alpha_2\beta_1$. *Blood* 1997; **89**:1235–1242.

34 Nakamura T, Jamieson GA, Okuma M, Kambayashi J, Tandon NN. Platelet adhesion to native type I collagen fibrils. Role of GPVI in divalent cation-dependent and -independent adhesion and thromboxane A_2 generation. *J Biol Chem* 1998; **273**:4338–4344.

35 Takahara K, Murray R, FitzGerald GA, FitzGerald DJ. The response to thromboxane A_2 analogues in human platelets. Discrimination of two binding sites linked to distinct effector systems. *J Biol Chem* 1990; **265**:6836–6844.

J BIOCHEM MOLECULAR TOXICOLOGY
Volume 17, Number 1, 2003

Increase of Lipid Peroxidation by Cisplatin in WI38 Cells but Not in SV40-Transformed WI38 Cells

Hsiu-Chuan Yen,[1] Chung-Yi Nien,[1] Hideyuki J. Majima,[2] Chia-Pei Lee,[1] Sz-Yun Chen,[1] Jeng-Shu Wei,[1] and Lai-Chu See[3]

[1]School of Medical Technology, Chang Gung University, Kwei-Shan, Tao-Yuan 333, Taiwan, Republic of China; E-mail: *yen@mail.cgu.edu.tw*
[2]Department of Radiology, Dental School, Kagoshima University, Kagoshima 890-8544, Japan
[3]Department of Public Health, Biostatistics Consulting Center, Chang Gung University, Kwei-Shan, Tao-Yuan 333, Taiwan, Republic of China

Received 8 July 2002; revised 28 October 2002; accepted 1 November 2002

ABSTRACT: Cisplatin (CPT) is an effective anticancer drug that causes cumulative toxicity to normal tissues. It has been suggested that CPT damages normal cells by causing oxidative stress, but it is not known whether it can induce similar oxidative damage to tumor cells. In this study, by using normal human lung fibroblast (W138) cells and SV40-transformed WI38 (VA13) cells as a model, we compared the effect of CPT on cytotoxicity, apoptosis, lipid peroxidation, and mitochondrial gene expression, which could be regulated by oxidative stress, between normal and tumor cells. CPT induced greater growth inhibition and percentage of apoptotic cells in VA13 cells. However, levels of esterified F_2-isoprostanes and 4-hydroxy-2-nonenal, two specific products of lipid peroxidation, were increased by CPT in WI38 cells, but not in VA13 cells. Furthermore, the transcript level of mitochondrial 12S rRNA was augmented by CPT in both cells, but to a higher degree in WI38 cells. The data suggest a correlation between lipid peroxidation and cytotoxicity or increased mitochondrial transcript levels in WI38 cells but not in VA13 cells. The results also indicate an altered response of oxidative damage and mitochondrial gene regulation to CPT in the transformed phenotype of WI38 cells.
 J Biochem Mol Toxicol 17:39–46, 2003; Published online in Wiley InterScience (www.interscience.wiley.com). DOI 10.1002/jbt.10059

KEYWORDS: **Cisplatin; F_2-Isoprostanes; 4-Hydroxy-2-nonenal; Lipid Peroxidation; Mitochondrial Gene Expression; Transformed Cells**

Correspondence to: Hsiu-Chuan Yen, Ph.D.
Contract Grant Sponsor: National Science Council, Taiwan.
Contract Grant Number: NSC 89-2314-B-182-070, NSC 89-2320-B-182-053, and NSC 90-2320-B-182-061.
Contract Grant Sponsor: Ministry of Education, Culture, Sports, Science and Technology, Japan.
Contract Grant Number: JGME 12671844.

INTRODUCTION

Cisplatin (CPT), or *cis*-dichlorodiammine platinum(II), is an important anticancer drug but its irreversible cumulative toxicity to normal tissue has been a major clinical problem during CPT therapy [1]. The chlorinated form of CPT becomes electrophilic once CPT gets hydrated inside the plasma membrane and can react with nucleophilic molecules such as DNA bases and sulfhydryl groups [2]. Although there is no known pathway by which CPT generates reactive oxygen species (ROS) directly, it has been proposed that oxidative stress is an important mechanism of CPT-induced normal tissue toxicity possibly due to depletion of glutathione (GSH) [2,3]. On the other hand, it has been shown that CPT inhibited the function of respiratory complexes in normal tubular cells [4]. Since mitochondrial respiratory chain is a source of ROS [5], mitochondrial damage could also be a source of oxidative stress induced by CPT. The use of antioxidants has therefore been proposed as a means to alleviate CPT-induced toxicity [6,7]. However, whether effects of CPT on redox status and mitochondria are similar between normal and tumor cells remains to be determined.

Lipid peroxidation is initiated by the abstraction of allylic hydrogen on polyunsaturated fatty acids (PUFAs) by free radicals. F_2-isoprostanes, a group of prostaglandin F_2 (PGF_2)-like compounds, are specific in vivo markers of lipid peroxidation produced from free-radical-catalyzed peroxidation of arachidonic acid independent of the cyclooxygenase pathway [8] and are initially formed in situ esterified to phospholipid on membranes [9]. 15-F_{2t}-isoprostane (15-F_{2t}-IsoP) or 8-iso-$PGF_{2\alpha}$, the most abundant form of F_2-isoprostanes in vivo, has been shown to be elevated in a variety of oxidative stress related human diseases and toxicity [10]. On the other hand, 4-hydroxy-2-nonenal (HNE) is formed during the peroxidation of ω6-PUFAs

by cleavage of lipid hydroperoxides catalyzed by transition-metal ions [11]. HNE is a highly reactive and toxic aldehyde that can react with GSH or macromolecules to form protein adducts, DNA adducts, and phospholipid adducts [12]. It has been shown that HNE can modulate the activity of redox-sensitive transcription factors [13], indicating the involvement of HNE in signal transduction pathways.

Human mitochondrial DNA (mtDNA) is a circular DNA with 16,569 bp. It encodes 13 polypeptides as essential subunits of complexes for oxidative phosphorylation, and 2 rRNA and 22 tRNA genes [14]. Nuclear DNA-encoded mitochondrial transcription factor A (mtTFA) is required for the transcription of mtDNA [15]. Oxidative stress has been suggested to modulate mitochondrial gene expression either by retrograde signaling from mitochondria to nucleus or through redox-sensitive transcription factors, such as nuclear respiratory factor-2 (NRF-2), AP-1, and NF-κB [16,17]. Upregulation of both nuclear and mtDNA genes for oxidative phosphorylation was found in adenine nucleotide translocator (ANT)-1 knockout mice with oxidative stress [18,19] and in human cells treated with antimycin A that induced oxidative stress by inhibiting respiratory complex III [20]. Furthermore, it has been shown that the upregulation of NRF-1, mtTFA, and NF-κB was associated with increased levels of hydrogen peroxide in mtDNA-depleted HeLa cells [21].

It has been indicated that the redox status differs between normal and tumor cells. For example, levels of Mn superoxide dismutase, a mitochondrial antioxidant enzyme that scavenges superoxide anion radicals, were reduced in transformed cells compared to their normal counterparts [22]. Some tumors had higher levels of GSH in tumor cells than in normal cells [23], or were less responsive to agents stimulating lipid peroxidation [24,25]. On the other hand, characteristics of mitochondria and energy metabolism were often altered in tumors, such as the change in respiratory functions and mitochondrial morphology [26]. It has been hypothesized that altered mitochondrial physiology, by affecting apoptosis and cell signaling through ROS, may play important roles in cellular transformation [17]. Therefore, responses of normal and tumor cells to oxidative stress induced by CPT may be different.

In this study, we compared the effect of CPT on cytotoxicity, apoptosis, lipid peroxidation, and mitochondrial 12S rRNA transcript levels in normal human WI38 cells and in SV40-transformed WI38 (VA13) cells. We show that CPT exerted different effects on levels of lipid peroxidation and mitochondrial 12S rRNA between WI38 and VA13 cells although CPT treatment resulted in greater growth-inhibitory effect and cell death in VA13 cells.

MATERIALS AND METHODS

Cell Culture

The embryonic human lung fibroblast WI38 cells (ATCC CCL 75) and their SV40-transformed subline VA13 cells (ATCC CCL 75.1) were obtained from Riken Cell Bank, Japan. The passage number of WI38 cells used in this study was 28–33. Both cells were maintained in minimum essential media (MEM) with Earl's salts supplemented with 10% defined fetal bovine serum (HyClone, UT). The use of WI38 and VA13 cells as counterparts to a cell model for comparing the difference between normal and tumor cells has been previously reported [27,28].

Cytotoxicity Assay

Cytotoxicity was evaluated by the growth inhibition. CPT was purchased from Bristol-Myers Squibb S.p.A. (Italy) in the form of 0.5 mg/mL solution (Plantinex). Cells grown in 96-well tissue culture plates were treated with various doses of CPT 48 h before confluence. At the end of treatment, cells were incubated with reagents from the CellTiter 96 Aqueous One Solution Cell Proliferation Assay Kit (Promega, WI). The absorbance of reduced tetrazolium compound catalyzed by dehydrogenases in viable cells was recorded at 490 nm. On the other hand, cell number in 6-well plates was also counted after 48-h CPT treatment at the dose of 6.7 μM (2 μg/mL) to verify results using the colorimetric kit.

Microscopic Assessment of Nuclear Chromatin Condensation and Fragmentation

Extent of apoptosis was quantified by the presence of nuclear chromatin and fragmentation by staining the nuclei of cells with Hoechst 33342 dye, using previously described methods [29,30]. Hoechst 33342 dye is a minor groove-binding dye that can easily enter cells during the early state of apoptosis [31]. Cells grown on glass-bottomed and poly-D-lysine coated 35-mm dishes (MatTek Corp., Ashland, MA) were fixed in 4% paraformaldehye in phosphate-buffered saline (PBS) for 30 min, washed with PBS, and then incubated with Hoechst 33342 dye (Molecular Probes, Eugene, OR) at the final concentration of 1 μg/mL for 30 min. Cells were washed twice with PBS and fluorescence of the dye was visualized by exciting the dye at 340 nm with an inverted microscope equipped with an UV epifluorescence filter (TE200, Nikon, Tokyo, Japan). Random fields were selected and 300–500 cells were

counted. Percentage of apoptotic cells was calculated for each dish.

Detection of Esterified F_2-isoprostanes

The extraction and purification of F_2-isoprostanes from samples was performed according to the method described by Morrow and Roberts [32]. All organic solvents were purchased from Merck (Darmstadt, Germany). Phospholipids in cells were extracted by homogenizing cells in ice-cold Folch solution (chloroform/methanol, 2:1 v/v) containing 0.005% butylated hydroxytoluene (BHT) and hydrolyzed with 15% KOH. The hydrolyzed free F_2-isoprostanes were purified by performing solid-phase extraction using C_{18} columns and silica columns from J.T. Baker (Phillipsburg, NJ) with a 24-channel vacuum manifold from J.T. Baker [33]. The nitrogen-dried eluate was resuspended in the enzyme immunoassay (EIA) buffer. 15-F_{2t}-IsoP was then analyzed by using an 8-isoprostane EIA kit from Cayman Chemical (Ann Arbor, MI). The standard curve and concentrations of unknown samples were plotted and calculated by using the 4-parameter fit in the softmax Pro software (Molecular Devices, Sunnyvale, CA). The level of 15-F_{2t}-IsoP was normalized by the cell number of each sample.

Detection of Intracellular HNE-Modified Proteins

This method has been previously described by Motoori et al. [30]. Cells grown on glass-bottomed dishes were fixed with 4% paraformaldehyde in PBS. Cell membranes were permeabilized by 95% ethanol plus 5% acetic acid. After being washed with PBS twice and then with PBS containing 0.1% bovine serum albumin (BSA) twice, cells were incubated with anti-HNE-modified protein monoclonal antibody (Japan Institute for the Control of Aging, Japan) at the concentration of 0.5 μg/mL for 60 min and finally incubated with AlexaFlour 488 goat anti-mouse IgG (H + L) secondary antibody (Molecular Probes) at the concentration of 10 μg/mL for 60 min. Fluorescent images were acquired and quantified using a CSU-10 confocal laser scanning unit (Yokogawa Electric Co., Tokyo, Japan) coupled to an LX90 inverted microscope (Olympus Optical Co.) and a C5810-1 color-chilled 3CCD camera (Hamamatsu Photonics K.K., Japan). The AlexaFlour 488 was excited at 488 nm and the emission was filtered using a 515-nm barrier filter. The intensity of the laser beam, the gain of the amplifier, and the exposure time were held at 500 μW, 18 dB, and 5 s respectively. The focus of the cells was adjusted to the middle of Z-axis before exposing the cells to laser and taking images. Therefore, each field taken was only exposed to the laser once. Several fields were scanned randomly. Fluorescent intensity per unit area of each field was quantified using IPLab Spectrum version 3.0 software (Scanalytics Inc., VA). Data were presented as the relative intensity calculated by dividing mean fluorescence intensity of each field with that of one data from the WI38 control group.

Nonradioactive Northern Blot Analysis

Total RNA was isolated by the StrataPrep Total RNA Miniprep Kit with DNase I treatment (Stratagene, La Jolla, CA). The concentration of RNA was determined by measuring the absorbance at 260 nm. The ratio of absorbance at 260 to that at 280 nm was at least 1.8. The level of mitochondrial 12S rRNA was detected by nonradioactive Northern blot analysis modified from the manufacturer's instruction (The DIG System User's Guide for Filter Hybridization, Roche, Mannheim, Germany). Fifteen micrograms of total RNA was electrophoresed in 1.5% agarose gel containing formaldehyde [34] and transferred to the GeneScreen Neutral Nylon membranes (NEN, Boston, MA) in 10× SSC (3 M sodium chloride and 300 mM sodium citrate, pH 7.0 for 20× SSC). Digoxigenin (DIG)-labeled probes for mitochondrial genes were generated by polymerase chain reaction (PCR) using total DNA isolated from WI38 cells as the template and the PCR DIG Probe Synthesis Kit (Roche). Primers for 12S rRNA were 5'CCCCATACCCCGAACCAACC3' and 5'GGAGTGGGTTTGGGGCTAGG3'. DIG-labeled probes for β-actin were also generated by PCR but using cDNA as the template and the primers 5'AGAGATGGCCACGGCTGCTT3' and 5'ATTTGCGGTGGACGATGGAGG3'. Membranes with RNA were placed in a UV cross-linker at 0.12 J/cm^2, prehybridized in hybridization solution (50% deionized formamide, 5× SSC, 0.1% *N*-lauroyl-sarcosine, 0.02% SDS, 2% blocking reagent from Roche) at 42°C for 1 h, and then hybridized with gel-purified probes in hybridization solution at 42°C overnight. The membranes were then washed twice in the first wash buffer (2× SSC and 0.1% SDS) at room temperature and in the second wash buffer (0.5× SSC and 0.1% SDS) at 68°C. The DIG on hybridized probes was detected by the DIG Luminescent Detection Kit (Roche) with alkaline phosphatase-conjugated anti-DIG antibody according to the manufacturer's instruction. Chemiluminescent bands were detected by exposing the membranes to the BioMax ML film (Kodak, Rochester, NY) and the density on the film was analyzed by the ChemiDoc system (Biorad, Hercules, CA) or directly photographed and analyzed by the ChemiDoc. Total RNA isolated from mtDNA-depleted

143B-TK$^-$ (143B-TK$^-$-ρ^0) cells, which were obtained from Dr. Douglas C. Wallace at Emory University [35], was used as a negative control in the Northern blot analysis.

Statistical Analysis

Data were analyzed by SAS Win 8.1 software (SAS Institute, Cary, NC). Two-way analysis of variance (ANOVA) was first used to examine the interaction between cell type (WI38 vs. VA13) and treatment (control vs. CPT), that is, to examine whether WI38 cells reacted to the treatment effect differently from the way VA13 cells reacted to the treatment effect. If interaction between cell type and treatment was significant, one-way ANOVA was further used to compare the difference among multiple groups. All data were presented as mean ± standard deviation (SD). Statistical significance was considered when $p < 0.05$.

RESULTS

Inhibition of Cell Growth and Induction of Apoptosis by CPT

To compare the effect of 48-h CPT treatment on the growth of WI38 and VA13 cells, cytotoxicity was first accessed by colorimetric method for a dose range (0.67–66.7 μM) of CPT, and the exact cell number remaining after CPT treatment was counted in both cells at the dose of 6.7 μM. As shown in Figure 1, there was significantly higher cytotoxicity in VA13 cells than in WI38 cells after 48-h CPT treatment in the range from 3.34 to 33.4 μM. The dose that inhibited 50% growth (IC_{50}) for WI38 and VA13 cells was approximately 51.3 and 5.7 μM of CPT, respectively. By counting the cell number directly, we confirmed that 6.7 μM (2 μg/mL) of CPT treatment resulted in greater reduction in cell growth in VA13 than WI38 cells, following 48-h treatment (Figure 2). There was 51 and 27% reduction in cell number by 48-h CPT treatment in WI38 and VA13 cells, respectively. To further evaluate the role of apoptosis in the reduction of cell number after CPT treatment, percentage of apoptotic cells following Hoechst 33342 staining were counted under a fluorescence microscope. Table 1 shows that CPT caused significant increase of apoptotic cells in both WI38 and VA13 cells and the effect was greater in VA13 cells.

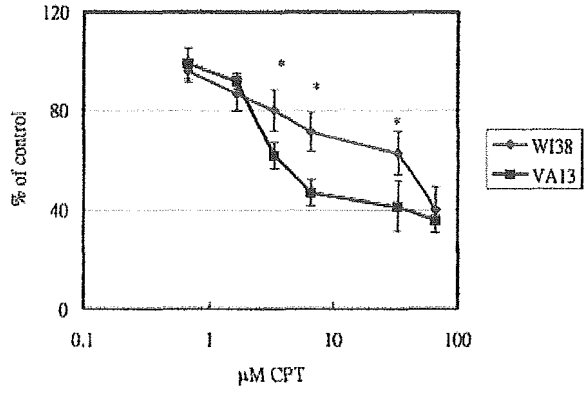

FIGURE 1. Cell proliferation assay for WI38 and VA13 cells treated with CPT for 48 h. Data were represented as percentage relative to mean of the control group ($n = 5$ for each group). The X-axis is in log scale.

Levels of Lipid Peroxidation

To compare lipid peroxidation after CPT treatment, cells were treated with CPT for 48 h at the dose of 6.7 μM and lipid peroxidation levels were measured. Figure 3 shows that levels of esterified 15-F_{2t}-IsoP were significantly increased in WI38 cells after CPT treatment, but not in VA13 cells. Furthermore, HNE-protein adducts were detected using immunofluorescent staining and the image is shown in Figure 4. Quantification of the fluorescent images indicated that intracellular levels of HNE were also elevated in WI38 cells, but not in VA13 cells (Table 2). These findings provided strong evidence for the occurrence of lipid peroxidation in WI38 cells

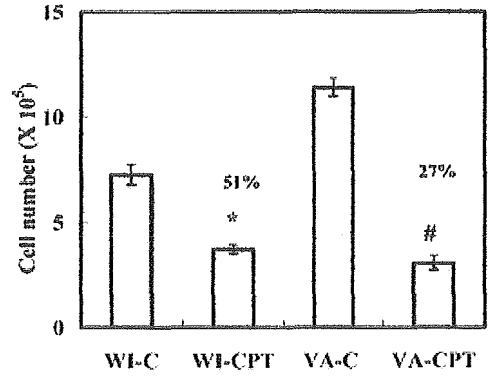

FIGURE 2. Cell count after 48-h CPT treatment. WI-C, control group of WI38 cells; WI-CPT, CPT (6.7 μM)-treated WI38 cells; VA-C, control group of VA13 cells; VA-CPT, CPT-treated VA13 cells. Two-way ANOVA was made ($n = 4$ for each group). Interaction between cell type and treatment was statistically significant ($p < 0.001$), indicating the reduction of cell number following CPT treatment was significantly different between WI38 cells (51% remained) and VA13 cells (27% remained). One-way ANOVA was further made and showed that CPT treatment resulted in significant inhibition of cell growth in either WI38 or VA13 cells. *, WI-CPT vs. WI-C ($p < 0.001$); #, VA-CPT vs. VA-C ($p = 0.03$).

TABLE 1. Microscopic Assessment of DNA Chromatin Condensation and Fragmentation by Hoechst 33342 Staining

Group	*Percentage of Apoptotic Cells*
WI38-control	0.616 ± 0.199
WI38-CPT	2.415 ± 0.702[a]
VA13-control	0.857 ± 0.458
VA13-CPT	5.053 ± 1.816[b]

Percentage of apoptotic cells were calculated from 300 to 500 cells counted. Data were obtained from four dishes for each group. Two-way ANOVA indicated significant interaction effect between cell type and treatment ($p = 0.03$). One-way ANOVA indicated that there was significant increase of percentage of apoptotic cells in either WI38 or VA13 cells.
[a] WI38-CPT vs. WI38-control ($p < 0.001$).
[b] VA13-CPT vs. VA13-control ($p = 0.003$).

as the results of F_2-isoprostanes and HNE agreed with each other.

Levels of 12S rRNA Relative to Nuclear β-actin mRNA

Since CPT can cause mitochondrial dysfunction [4] and mtDNA damage [36], we next determined the pattern of mitochondrial gene expression, which could be modulated by oxidative stress or mitochondrial dysfunction. We established nonradioactive Northern blot analysis using PCR-generated and DIG-labeled probes to detect steady-state RNA levels. Figure 5A shows the excellent quality of total RNA of each sample following electrophoresis. Figure 5B shows levels of mitochondrial 12S rRNA and β-actin mRNA from nucleus. After normalization to the density of β-actin bands in arbitrary densitometric units, levels of 12S rRNA gene were increased by 203 ± 52% and 132.5 ± 3%, relative to the control group, in WI38 and VA13 cells respectively, following CPT treatment from three sets of experiments, but the increase in WI38 was more.

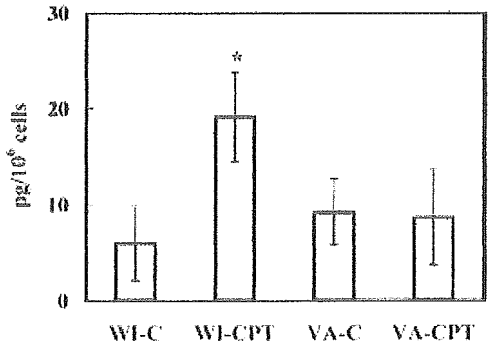

FIGURE 3. Levels of esterified 15-F_{2t}-IsoP in WI38 and VA13 cells. Cells were treated with 6.7 μM of CPT for 48 h. Data were represented as mean ± SD (n = 5–6 for each group). *, CPT-treated WI38 cells had significantly higher level of esterified 15-F_{2t}-IsoP than its control cells ($p = 0.001$). WI-C, WI-CPT, VA-C, and VA-CPT represent the same groups described in Figure 2.

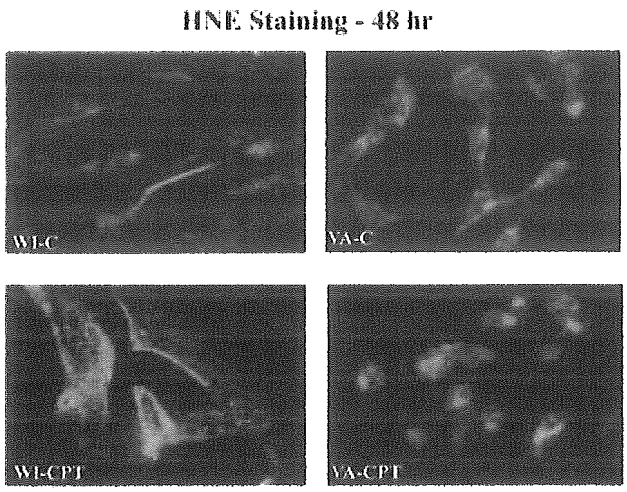

FIGURE 4. Immunofluorescent staining for detecting intracellular levels of HNE-protein adducts in cells. WI-C, WI-CPT, VA-C, and VA-CPT represent the same groups described in Figure 2.

DISCUSSION

We have shown that in spite of inducing greater growth inhibition and apoptosis in VA13 cells than in WI38 cells, CPT increased lipid peroxidation in WI38 cells but not in VA13 cells, indicating a differential response in transformed phenotypes. The results indicate that although CPT, as an anticancer drug, unsurprisingly has more greater inhibitory effect on the growth of VA13 cells, which have faster proliferation rate, it can preferentially cause oxidative damage to normal WI38 cells by inducing lipid peroxidation. We have also demonstrated that CPT could have a positive effect on transcription of mtDNA, and the increase of 12S rRNA in WI38 cells was greater than that in VA13 cells.

Because much lower doses of CPT and a longer treatment time were used in the current study, the results would be different from that of experiments using much higher acute doses [4,6]. There was no appreciable amount of lactate dehydrogenase released in the medium following the CPT treatment (data not shown). Although CPT also significantly increased the amount

TABLE 2. Quantification of Intracellular HNE Levels

Group	*Relative HNE Levels*
WI38-control	1.00 ± 0.05
WI38-CPT	1.23 ± 0.11[a]
VA13-control	1.08 ± 0.11
VA13-CPT	1.11 ± 0.08

Data were presented the ratio of relative fluorescence intensity to one WI38 control data. There were 13–15 data from three dishes for each group. The intracellular levels of HNE-protein adducts were significantly increased by CPT in WI38 cells but not in VA13 cells.
[a] WI38-CPT vs. WI38-control group ($p < 0.001$).

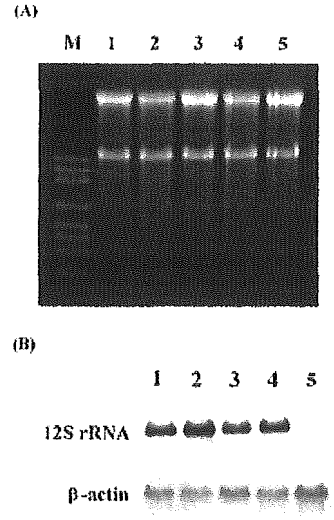

FIGURE 5. Northern blot analysis for the detection of mitochondrial 12S rRNA transcript level. RNA gel electrophoresis showed excellent quality of total RNA (A). Steady-state levels of mitochondrial 12S rRNA and nuclear β-actin mRNA in WI38 and VA13 cells before and after 48-h CPT treatment were shown (B). M, 0.16–1.77 Kb RNA ladder from GIBCO; 1, WI38 control; 2, CPT-treated WI38; 3, VA13 control; 4, CPT-treated VA13; 5, 143-B-TK$^-$-ρ^0 cells.

of apoptotic cells, there was only about 2.4 and 5.1% of apoptotic cells in CPT-treated WI38 and VA13 cells, respectively (Table 1). The results indicate that such small degree of apoptosis may contribute to greater cytotoxicity in VA13 cells but its significance was uncertain since degree of growth inhibition was much higher (Figure 2). Although it is known that oxidative stress is important in apoptosis [37], the results suggest that apoptosis induced by CPT in VA13 cells may not be associated with lipid peroxidation.

Detection of lipid peroxidation provides one reliable indicator for the occurrence of oxidative damage to cells. Most studies showing CPT-mediated lipid peroxidation applied a less specific indicator of lipid peroxidation, malondialdehyde [3]. In our study, we used two more specific markers of lipid peroxidation. There was one report showing that CPT treatment increased F_2-isoprostanes in normal renal tubular cells [6]. By using a much lower dose, we also showed an increase in F_2-isoprostanes levels in normal WI38 cells. In addition to F_2-isoprostanes, elevation of intracellular cytotoxic HNE was also found in WI38 cells following CPT treatment, which was first demonstrated in CPT toxicity by our study. We also first demonstrated preferential increase in lipid peroxidation levels by CPT in normal WI38 cells but not their transformed counterpart cells. It has been shown that HNE could not only activate NF-κB and induce apoptosis, but also further induce the formation of 15-F_{2t}-IsoP in normal cells [38]. There were many possible explanations as to how CPT caused lipid peroxidation in WI38 but not in VA13 cells. First, if GSH depletion was the major cause of lipid peroxidation, VA13 cells could have more protection because of higher total glutathione levels [27]. Increased formation of HNE in WI38 cells could further augment GSH depletion. However, as with the action of many anticancer drugs, CPT-mediated DNA damage by forming interstrand cross-links with DNA [39] may have a more detrimental effect on the growth of VA13 cells because of more active proliferating ability of VA13 cells. Second, if lipid peroxidation was initiated from mitochondria, the difference in the outcome of oxidative stress between WI38 and VA13 cells could be due to possible altered mitochondrial properties in VA13 cells, which requires further examination. Finally, there could be an altered lipid composition, such as the proportion of arachidonic acids, or altered metabolism and regulation of fatty acids in VA13 cells. As reviewed by Dianzani [24], normal liver and hepatoma cells generally have different levels and compositions of PUFAs. AH-130 Yoshida ascites tumors were much less responsive to stimulation that induced lipid peroxidation than were normal hepatocytes, but enrichment of arachidonic acids resulted in the restoration of the lipid peroxidation responses in hepatoma cells.

We have also demonstrated that CPT can augment steady-state levels of mitochondrial 12S rRNA. Since the formation of individual mitochondrial transcripts is generated from the same initial polycistronic transcript, which is controlled by mtTFA from the nucleus [15,40], only 12S rRNA transcript levels were examined. It has been shown that the upstream region of mtTFA gene has recognition sites for NRF-1, NRF-2, and Sp1 [41], which could be regulated by redox signaling [17]. It is possible that CPT can damage mtDNA via oxidative damage or by direct cross-linking [35,38]. It has been demonstrated that there was increased expression of both mitochondrial and nuclear genes associated with oxidative phosphorylation in tissues of patients carrying genetic mtDNA mutations [42]. Therefore, CPT may increase mitochondrial transcription by altering activities of nuclear-encoded transcription factors in response to oxidative stress, metabolic signals, or mtDNA damage. Furthermore, because HNE detected was bound to proteins and HNE may modulate the activity of redox-sensitive transcription factors [13,38], it is also possible that HNE can affect factors regulating mitochondrial gene expression. Higher lipid peroxidation levels in WI38 cells may contribute to the higher degree of 12S rRNA increase in WI38 cells than in VA13 cells. Possible different mitochondrial properties or regulatory mechanisms of mitochondrial genes between WI38 and VA13 cells may also contribute to this difference.

In conclusion, we have shown that CPT significantly increased levels of lipid peroxidation in WI38 cells, but not in VA13 cells. Our results suggest that CPT may preferentially induce lipid peroxidation in normal cells independent of the extent of growth inhibition and apoptosis or lipid peroxidation is less inducible by CPT in tumor cells. Nevertheless, the increase of lipid peroxidation would have toxic effects on normal cells by interfering normal membrane functions on cell membrane or intracellular organelles, such as mitochondria. Moreover, the higher increase of mitochondrial transcripts by CPT in WI38 cells may be associated with higher levels of lipid peroxidation in WI38 cells. These findings may have implications in managing CPT-induced toxicity by understanding the differential responses between normal and transformed cells to CPT.

ACKNOWLEDGMENT

We thank Ms. Chizuru Yamaguchi and Dr. Shizuko Kakinuma for helpful technical assistance.

REFERENCES

1. Cvitkovic E. Cumulative toxicities from cisplatin therapy and current cytoprotective measures. Cancer Treatment Rev 1998;24:265–281.
2. Hacker M. Toxicity of platinum-based anticancer drugs. In: Powis G, Hacker HP, editors. The Toxicity of Anticancer Drugs. New York: Pergamon Press; 1991. pp 82–105.
3. Kharbangar A, Khynriam D, Prasad SB. Effect of cisplatin on mitochondrial protein, glutathione, and succinate dehydrogenase in Dalton lymphoma-bearing mice. Cell Biol Toxicol 2000;16:3636–373.
4. Kruidering M, van de Water B, de Heer E, Mulder GJ, Nagelkerke JF. Cisplatin-induced nephrotoxicity in porcine proximal tubular cells: Mitochondria dysfunction of complex I to IV of the respiratory chain. J Pharmacol Exp Ther 1997;280:638–649.
5. Richter C, Gogvadze V, Laffranchi R, Schlabach R, Schweizer M, Suter M, Walter P, Yaffee M. Oxidants in mitochondria: From physiology to diseases. Biochim Biophys Acta 1995;1271:67–74.
6. Salahudeen A, Poovala V, Parry W, Pande R, Kanji V, Ansari N, Morrow J, Roberts J II. Cisplatin induced *N*-acetyl cysteine suppressible F_2-isoprostane production and injury in renal tubular epithelial cells. J Am Soc Nephrol 1998;9;1448–1455.
7. Rybak LP, Husain K, Whitworth C, Somani SM. Dose dependent protection by lipoic acid against cisplatin-induced ototoxicity in rats: antioxidant defense system. Toxicol Sci, 1999;47:195–202.
8. Morrow JD, Hill KE, Burk RF, Nammour RM, Badr KF, Roberts LJ II. A series of prostaglandin F_2-like compounds are produced in vivo in humans by a non-cyclooxygenase, free radical-catalyzed mechanism. Proc Natl Acad Sci USA 1990;87:9383–9387.
9. Morrow JD, Awad JA, Boss HJ, Blair IA, Roberts LJ II. Non-cyclooxygenase-derived prostanoids (F_2-isoprostanes) are formed in situ on phospholipids. Proc Natl Acad Sci USA 1992;89:10721–10725.
10. Roberts LJ II, Morrow JD. Measurement of F_2-isoprostanes as an index of oxidative stress in vivo. Free Radic Biol Med 2000;28:505–513.
11. Halliwell B, Gutteridge JMC. Free Radicals in Biology and Medicine, 3rd edition. New York: Oxford University Press; 1999. 936 p.
12. Esterbauer H, Schaur RJ, Zollner H. Chemistry and biochemistry of 4-hydroxynonenal, malonaldehyde and related aldehydes. Free Radic Biol Med 1991;11:81–128.
13. Leonarduzzi G, Arran MC, Basaga H, Chiarpotto E, Sevanian A, Poli G. Lipid oxidation products in cell signaling. Free Radic Biol Med 2000;28:1370–1378.
14. Wallace DC. Mitochondrial diseases in man and mouse. Science 1999;283:1482–1488.
15. Moraes C. What regulates mitochondrial DNA copy number in animal cell? Trends Genet 2001;17:199–205.
16. Poyton RO. Crosstalk between nuclear and mitochondrial genomes. Annu Rev Biochem 1996;65:563–607.
17. Preston TJ, Abadi A, Wilson L, Singh G. Mitochondrial contributions to cancer cell physiology: Potential for drug development. Adv Drug Delivery Rev 2001;49:45–61.
18. Esposito LA, Melov S, Panov A, Cotrell BA, Wallace DC. Mitochondrial disease in mouse results in increased oxidative stress. Proc Natl Acad Sci USA 1999;96:4820–4825.
19. Murdock DG, Boone BE, Esposito LA, Wallace DC. Up-regulation of nuclear and mitochondrial genes in the skeletal muscle of mice lacking the heart/muscle isoform of the adenine nucleotide translocator. J Biol Chem 1999;274:14429–14433.
20. Suzuki H, Kumagai T, Goto A, Sugiura T. Increase in intracellular hydrogen peroxide and upregulation of a nuclear respiratory gene evoked by impairment of mitochondrial electron transfer in human cells. Biochem Biophys Res Commun 1998;249:542–545.
21. Miranda S, Foncea R, Guerrero J, Leighton JF. Oxidative stress and upregulation of mitochondrial biogenesis genes in mitochondrial DNA-depleted HeLa cells. Biochem Biophys Res Commun 1999;258:44–49.
22. Oberley LW, Buettner GR. Role of superoxide dismutase in cancer. Cancer Res 1979;39:1141–1149.
23. Russo A, DeGraff W, Friedman N, Mitchell JB. Selective modulation of glutathione levels in human normal versus tumor cells and subsequent differential response to chemotherapy drugs. Cancer Res 1986;46:2845–2848.
24. Dianzani MU. Lipid peroxidation and cancer: A critical reconsideration. Tumori 1989;75:351–357.
25. Jones GRN. Cancer destruction in vivo through disrupted energy metabolism part II. Lipid peroxidation and cell death; drug resistance as a consequence of reversible cellular injury. Physiol Chem Phys & Med NMR 1992;24:181–194.
26. Pederson PL. Tumor mitochondria and the biogenetics of cancer cells. Prog Exp Tumor Res 1978;22:190–274.
27. Wan XS, Clair DK. Differential cytotoxicity of buthionine sulfoximine to "normal" and transformed human lung fibroblast cells. Cancer Chemother Pharmacol 1993;33:210–214.
28. Chen ZP, Schell JB, Ho C-T, Chen KY. Green tea epigallocatechin gallate shows a pronounced growth inhibitory effect on cancerous cells but not on their normal counterparts. Cancer Lett 1998;129:173–179.

29. Majima HJ, Oberley TD, Furukawa K, Mattson MP, Yen H-C, Szweda LI, St. Clair DK. Prevention of mitochondrial injury by manganese superoxide dismutase reveals a primary mechanism for alkaline-induced cell death. J Biol Chem 1998;273:8217–8224.
30. Motoori S, Majima HJ, Ebara M, Kato H, Hirai F, Kakinuma S, Yamaguchi C, Ozawa T, Nagano T, Tsujii H, Saisho H. Overexpression of mitochondrial manganese superoxide dismutase protects against radiation-induced cell death in the human hepatocellular carcinoma cell line HLE. Cancer Res 2001;61:5382–5388.
31. Haugland RP. Handbook of Fluorescent Probes and Research Products, Web edition (www.probes.com/handbook). Eugene, OR: Molecular Probes, Inc; 2002.
32. Morrow JD, Roberts LJ II. F_2-isoprostanes: Prostaglandin-like products of lipid peroxidation. In: Punchard NA, Kelly FJ, editors. Free Radicals. A Practical Approach. New York: Oxford University Press; 1996. pp 147–157.
33. Yen H-C, Cheng H-S, Hsu Y-T, Ho H-J, Nien C-Y, Lee Y-S. Effects of age and health status on levels of urinary 15-F_{2t}-isoprostane. J Biomed Lab Sci 2001;13:24–28.
34. Sambrook J, Russell DW. Molecular Cloning. A Laboratory Manual, 3rd edition. Cold Spring Harbor, New York: Cold Spring Harbor Laboratory Press; 2001.
35. Trounce I, Schmiedel J, Yen H-C, Hosseini S, Brown MD, Olson JJ, Wallace DC. Cloning of neuronal mtDNA variants in cultured cells by synaptosome fusion with mtDNA-less cells. Nucleic Acids Res 2000;28:2164–2170.
36. Olivero OA, Chang PK, Lopez-Larraza DM, Semino-Mora MC, Poirier MC. Preferential formation and decreased removal of cisplatin-DNA adducts in Chinese hamster ovary cell mitochondrial DNA compared to nuclear DNA. Mutat Res 1997;391:79–86.
37. Chandra J, Samali A, Orrenius S. Triggering and modulation of apoptosis by oxidative stress. Free Radic Biol Med 2000;29:323–333.
38. Ruef J, Moser M, Bode C, Kubler W, Runge MS. 4-Hydroxylnonenal induced apoptosis, NF-κB-activation and formation of 8-isoprostane in vascular smooth muscle cells. Basic Res Cardiol 2001;96:143–150.
39. Zou Y, van Houten B, Farrell N. Sequence specificity of DNA–DNA interstrand cross-link formation by cisplatin and dinuclear platinum complexes. Biochemistry 1994;33:5405–5410.
40. Attardi G. Biogenesis of mitochondria. Ann Rev Cell Biol 1988;4:289–333.
41. Virbasius JV, Scarpulla RC. Activation of human mitochondrial transcription factor A gene by nuclear respiratory factors: A potential link between nuclear and mitochondrial gene expression in organelle biogenesis. Proc Natl Acad Sci USA 1994;92:1309–1313.
42. Heddi A, Stepien G, Benke PJ, Wallace DC. Coordinate induction of energy gene expression in tissues of mitochondrial disease patients. J Biol Chem 1999;274:22968–22976.

THE JOURNAL OF BIOLOGICAL CHEMISTRY
Vol. 278, No. 5, Issue of January 31, pp. 3170–3175, 2003
Printed in U.S.A.

Development of Novel Fluorescence Probes That Can Reliably Detect Reactive Oxygen Species and Distinguish Specific Species*[S]

Received for publication, September 10, 2002, and in revised form, October 28, 2002
Published, JBC Papers in Press, November 4, 2002, DOI 10.1074/jbc.M209264200

Ken-ichi Setsukinai‡, Yasuteru Urano‡, Katsuko Kakinuma§, Hideyuki J. Majima¶, and Tetsuo Nagano‡‖

From the ‡Graduate School of Pharmaceutical Sciences, The University of Tokyo, Hongo, Bunkyo-ku, Tokyo 113-0033, Japan, the §Biophotonics Research Project/MMBS, Graduate School of Science, The University of Tokyo, Misaki, Miura, Kanagawa 238-0225, Japan, and the ¶Kagoshima University Dental School, Sakuragaoka, Kagoshima, Kagoshima 890-8544, Japan

We designed and synthesized 2-[6-(4′-hydroxy)phenoxy-3*H*-xanthen-3-on-9-yl]benzoic acid (HPF) and 2-[6-(4′-amino)phenoxy-3*H*-xanthen-3-on-9-yl]benzoic acid (APF) as novel fluorescence probes to detect selectively highly reactive oxygen species (hROS) such as hydroxyl radical (·OH) and reactive intermediates of peroxidase. Although HPF and APF themselves scarcely fluoresced, APF selectively and dose-dependently afforded a strongly fluorescent compound, fluorescein, upon reaction with hROS and hypochlorite ($^-$OCl), but not other reactive oxygen species (ROS). HPF similarly afforded fluorescein upon reaction with hROS only. Therefore, not only can hROS be differentiated from hydrogen peroxide (H_2O_2), nitric oxide (NO), and superoxide (O_2^-) by using HPF or APF alone, but $^-$OCl can also be specifically detected by using HPF and APF together. Furthermore, we applied HPF and APF to living cells and found that HPF and APF were resistant to light-induced autoxidation, unlike 2′,7′-dichlorodihydrofluorescein, and for the first time we could visualize $^-$OCl generated in stimulated neutrophils. HPF and APF should be useful as tools to study the roles of hROS and $^-$OCl in many biological and chemical applications.

Reactive oxygen species (ROS)[1] play key roles in many pathogenic processes, including carcinogenesis (1), inflammation (2), ischemia-reperfusion injury (3), and signal transduction (4–7). Several methods, including electron spin resonance (8) and chemiluminescence (9), have been developed to detect ROS, but fluorescence detection is superior in terms of high sensitivity and experimental convenience. Experimental studies on Ca^{2+}-dependent signal transduction in cells were greatly facilitated by the development of fluorescent indicators for cytosolic Ca^{2+} (10, 11). Several fluorescence probes to detect ROS, such as 2′,7′-dichlorodihydrofluorescein (DCFH) and dihydrorhodamine 123, have also been developed. However, as Hempel and co-workers (12) pointed out, DCFH and dihydrorhodamine 123 can react with various ROS and oxidizing species (superoxide (O_2^-), hydrogen peroxide (H_2O_2), nitric oxide (NO), ferrous ion, and others), and in addition, DCFH is easily autoxidized, resulting in a spontaneous increase in fluorescence upon exposure to light. Therefore, it is not appropriate to think of these probes as detecting a specific oxidizing species in cells, such as H_2O_2 or NO, but rather they should be considered as detecting a broad range of oxidizing reactions that may be increased during intracellular oxidative stress (12).

There are many species of ROS, as mentioned above, but they tend to be considered collectively as "oxidative stress" when their effects in living cells are discussed. However, we believe that each species of ROS is likely to have a specific role in living cells. There is some evidence for this view. For example, H_2O_2 is an endothelium-derived hyperpolarizing factor in human and mice (13), p38 mitogen-activated protein kinase mediates caspase-3 activation during apoptosis induced by singlet oxygen ($^1O_2$) but not by H_2O_2 (14), and hydroxyl radical (·OH) plays an important role as a second messenger in T cell activation (15). In addition, each species of ROS has a characteristic chemical reactivity; for example, $^1O_2$ reacts with anthracenes to yield endoperoxides in the Diels-Alder mode (16), whereas ·OH can react directly with aromatic rings to yield hydroxylated products (17), and NO reacts with guanine to yield the deaminated compound (18). However, because of the problems, *i.e.* lack of selectivity among species and autoxidation (12, 19–20), the roles of an individual species of ROS in living cells remain uncertain. Therefore, we believe that it is very important to be able to detect each species of ROS selectively. If novel fluorescence probes that overcome the above problems were available, they would contribute greatly to the elucidation of the roles of individual ROS in living cells, because we would be able to "see" the generation of specific ROS with high resolution in time and space.

It is known that ·OH participates in various biological processes. For example, HeLa, MW451, and HL-60 cells are induced to undergo apoptosis by ·OH (21). ·OH can damage DNA bases (1) and mediates redox alteration of cell-membrane Ca^{2+} channels (22). However, because of the lack of effective direct detection methods for ·OH, its participation in these events has been established only indirectly by using inhibitors such as dithioethanol, glutathione, and desferrioxamine (1, 15, 21, 22).

* This work was supported by Ministry of Education, Science, Sports and Culture of Japan Research Grants 11794026, 12470475, 12557217 (to T. N.), 10771238 and 12771349 (to Y. U.). The costs of publication of this article were defrayed in part by the payment of page charges. This article must therefore be hereby marked "*advertisement*" in accordance with 18 U.S.C. Section 1734 solely to indicate this fact.

[S] The on-line version of this article (available at http://www.jbc.org) contains text and additional references.

‖ To whom correspondence should be addressed. Tel.: 81-3-5841-4850; Fax: 81-3-5841-4855; E-mail: tlong@mol.f.u-tokyo.ac.jp.

[1] The abbreviations used are: ROS, reactive oxygen species; DCFH, 2′,7′-dichlorodihydrofluorescein; HPF, 2-[6-(4′-hydroxy)phenoxy-3*H*-xanthen-3-on-9-yl]benzoic acid; APF, 2-[6-(4′-amino)phenoxy-3*H*-xanthen-3-on-9-yl]benzoic acid; HRP, horseradish peroxidase; PMA, 4β-phorbol-12-myristate-13-acetate; DCFH-DA, 2′,7′-dichlorodihydrofluorescein diacetate; Amplex Red, 10-acetyl-3,7-dihydroxyphenoxazine; HPPA, 3-(4-hydroxyphenyl)propionic acid; MPO, myeloperoxidase; DMF, *N*,*N*-dimethylformamide; HLE, human hepatocellular carcinoma cell line; CCD, charge coupled device; hROS, highly reactive oxygen species; ROO·, alkylperoxyl radical; NO, nitric oxide; O_2^-, superoxide radical.

Therefore, we wished to develop novel fluorescence probes for highly reactive oxygen species (hROS). Here, we use the term hROS to indicate reactive oxygen species with strong oxidizing power sufficient to directly hydroxylate aromatic rings (for example, ·OH or reactive intermediates of peroxidase).

We report herein the development of novel fluorescence probes for ROS, 2-[6-(4′-hydroxy)phenoxy-3*H*-xanthen-3-on-9-yl]benzoic acid (HPF) and 2-[6-(4′-amino)phenoxy-3*H*-xanthen-3-on-9-yl]benzoic acid (APF), which can specifically detect certain species of ROS in terms of an increase of fluorescence and exhibit complete resistance to autoxidation both *in vitro* and *in vivo*. We also describe the visualization of hypochlorite ($^-$OCl) in stimulated neutrophils.

EXPERIMENTAL PROCEDURES

Materials—4-Fluoronitrobenzene, 4-iodophenol, isobutene, 2,2,2-trifluoroethanol, and trifluoromethanesulfonic acid were purchased from Tokyo Kasei Kogyo Co., Ltd. (Tokyo, Japan). Uranine (sodium fluorescein), cuprous chloride, 2,2′-azobis(2-amidinopropane)dihydrochloride, horseradish peroxidase (HRP, EC 1.11.1.7), polyvinylpyrrolidone, and 4β-phorbol-12-myristate-13-acetate (PMA) were purchased from Wako Pure Chemical Industries Co., Ltd. (Osaka, Japan). Fluorescein was purchased from Aldrich. DCFH-DA and 10-acetyl-3,7-dihydroxyphenoxazine (Amplex Red) were purchased from Molecular Probes (Eugene, OR). 3-(4-Hydroxyphenyl)propionic acid (HPPA) was purchased from Dojindo Laboratories (Kumamoto, Japan). Myeloperoxidase (MPO, EC 1.11.1.7) was purchased from Calbiochem (San Diego, CA). Pyridine, dichloromethane, dimethyl sulfoxide (Me_2SO), and methanol were used after distillation. Other materials were of the best grade available and used without further purification.

Instruments—^{1}H NMR spectra were recorded on a JEOL JNM-LA300 instrument at 300 MHz. Mass spectra were determined with a JEOL JMS-SX102A mass spectrometer. Fluorescence spectroscopic studies were performed on a Hitachi F4500.

Fluorometric Analysis—The slit width was 2.5 nm for both excitation and emission. The photomultiplier voltage was 950 V. HPF, APF, and DCFH-DA were dissolved in DMF to obtain 10 mM stock solutions. We obtained DCFH by hydrolyzing DCFH-DA with 0.01 M aqueous NaOH for 30 min at 37 °C in the dark (12).

Cell Lines—A human hepatocellular carcinoma cell line (HLE) was purchased from the Health Science Research Resources Bank of Japan Health Sciences Foundation (Osaka, Japan). PCR3.1-Uni plasmid (Invitrogen) containing a sense human manganase-superoxide dismutase cDNA insert was a kind gift of Dr. Makoto Akashi (National Institute of Radiological Sciences, Chiba, Japan). The HLE cell line was transfected using the GenePORTER transfection procedure (Gene Therapy Systems, San Diego, CA) according to the previous report by Motoori and co-workers (23). Manganase-superoxide dismutase-transfected HLE cells were maintained in Dulbecco's modified Eagle's medium containing 10% fetal bovine serum (JRH Biosciences, Lenexa, KS) and 500 μg/ml Genetecin at 37 °C in humidified air containing 5% CO_2. Genetecin was removed at least 24 h before the experiments were performed.

Light-induced Autoxidation—Manganase-superoxide dismutase-transfected HLE cells were seeded 1 day before dye loading onto a glass-bottomed dish. The cells were then rinsed with modified Hanks' balanced salt solution containing 10.0 mM HEPES, 1.0 mM $MgCl_2$, 2.0 mM $CaCl_2$, and 2.7 mM glucose adjusted to pH 7.3 ± 0.05. Then, the cells were loaded with HPF or DCFH-DA (10 μM) by incubation for 30 min at 37 °C in the dark. Fluorescence images were acquired using a CSU-10 confocal laser scanning unit (Yokogawa Electric Co., Tokyo, Japan) coupled to an IX90 inverted microscope with an UPlanAPO ×20 objective lens (Olympus Optical Co.) and a C5810-01 color chilled 3CCD camera (Hamamatsu Photonics K. K.). The excitation wavelength was 488 nm, and the emission was filtered using a 515-nm barrier filter. After loading the dyes, the fluorescence images were acquired. After that, the cells were laser-irradiated at 488 nm for 10 s, and then the fluorescence images were acquired again. The laser power, the exposure time of the 3CCD camera (for acquiring the fluorescence images), and the gain of the amplifier were held at 500 μW, 1 s, and 18 decibels, respectively, to allow quantitative comparisons of the relative fluorescence intensity of the cells between groups.

Preparation of Porcine Neutrophils—Neutrophils were obtained from 1.8 liters of porcine blood basically according to the method of Wakeyama and co-workers (24) with some modifications (25). Erythrocytes in the buffy coat collected from blood were hemolyzed with a large volume of ice-cold 0.2% NaCl solution for 30 s, and then the preparation was promptly mixed with an equal volume of ice-cold 1.6% NaCl solution to restore the isotonic condition. Neutrophils were separated from platelets and mononuclear cells by the Conray-Ficoll method described previously (26). The neutrophils were suspended in Krebs-Ringer phosphate buffer (114 mM NaCl, 4.6 mM KCl, 2.4 mM $MgSO_4$, 1.0 mM $CaCl_2$, 15 mM NaH_2PO_4/Na_2HPO_4, pH 7.4) and kept on ice until use.

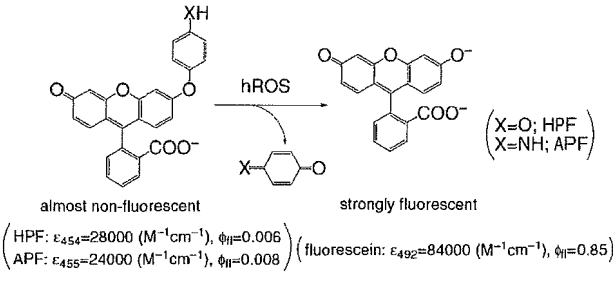

FIG. 1. **Scheme of *O*-dearylation reaction of HPF and APF with hROS.** ε is the molar absorptivity, and ϕ_{II} is the relative quantum efficiency of fluorescence.

Bioimaging of Neutrophils—Separated porcine neutrophils were seeded onto a glass-bottomed dish. Then, the cells were loaded with HPF or APF (10 μM) by incubation for 30 min at room temperature. Dye-loaded neutrophils were stimulated with PMA (2 ng/ml; 0.1% DMF was contained as a cosolvent). Fluorescence images were acquired twice in each experiment (before and 10 min after the stimulation with PMA) using an LSM510 confocal laser scanning unit (Carl Zeiss Co., Ltd.) coupled to an Axiovert 100M inverted microscope with a Plan-Neofluar ×100/1.3 objective lens (Carl Zeiss Co., Ltd.). The excitation wavelength was 488 nm, and the emission was filtered using a 505–550 nm barrier filter.

RESULTS

Design and Synthesis of HPF and APF—We reported previously that aryloxyphenols are *O*-dearylated in the *ipso*-substitution manner by hROS such as ·OH, reactive intermediates of peroxidase, and cytochrome P450, but not by other ROS ($O_2^{\cdot-}$, H_2O_2, $^1O_2$, and so on) (27, 28). In addition, our recent investigation of the absorption and fluorescence properties of fluorescein derivatives showed that the fluorescence of fluorescein could be quenched by protection of the phenolic hydroxy group at the 6′-position of fluorescein with an electron-rich aromatic ring.[2] Therefore, we designed and synthesized two novel fluorescence probes for hROS, HPF and APF, by making use of this fact. We expected that almost nonfluorescent HPF and APF would be *O*-dearylated upon reaction with hROS to yield strongly fluorescent fluorescein. The putative reaction scheme is shown in Fig. 1. The dynamic range of fluorescence augmentation should be wide, because both molar absorptivity and quantum efficiency values are greatly increased upon *O*-dearylation, so these compounds should operate as sensitive and selective fluorescence probes for hROS. HPF and APF were obtained in only 3 steps and 2 steps, respectively (see Supplemental Materials).

Reactivity of HPF and APF with ·OH—First, we investigated the reactivity of HPF and APF for chemically generated hROS. We tried to detect ·OH, one of the hROS, formed in the Fenton reaction, using HPF and APF (Fig. 2A). H_2O_2 was added to buffer solutions of HPF and APF and then ferrous perchlorate was added. The fluorescence intensity did not increase upon the addition of H_2O_2 alone, but increased substantially upon the addition of ferrous perchlorate in the presence of H_2O_2. The results clearly showed that both HPF and APF could detect ·OH selectively. In addition, the fluorescence increase caused by the reaction with ·OH was suppressed in buffer solutions of HPF and APF containing Me_2SO (a quencher of ·OH), and we confirmed the production of fluorescein in the reaction mixture with ·OH by reverse-phase high-performance liquid chromatog-

[2] K. Setsukinai, Y. Urano, and T. Nagano, manuscript in preparation.

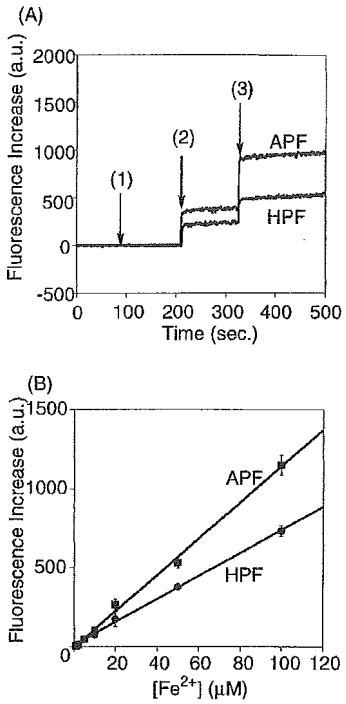

FIG. 2. **Detection of ·OH in the Fenton reaction using HPF and APF.** *A*, HPF (*lower line*) or APF (*upper line*) (final 10 μM; 0.1% DMF as a cosolvent) were added to sodium phosphate buffer (0.1 M, pH 7.4). The fluorescence intensity was determined at 515 nm with excitation at 490 nm. H_2O_2 (final 1 mM) was added at *1*, and ferrous perchlorate (final 100 μM) was added two times at *2* and *3*. *B*, relation between the concentrations of added ferrous perchlorate and fluorescence increase in the Fenton reaction. Data are mean ± S.E. (n = 3). HPF (*circle*) or APF (*square*) (final 10 μM; 0.1% DMF as a cosolvent) were added to sodium phosphate buffer (0.1 M, pH 7.4) containing H_2O_2 (1 mM). The wavelength for measurement was the same as *A*.

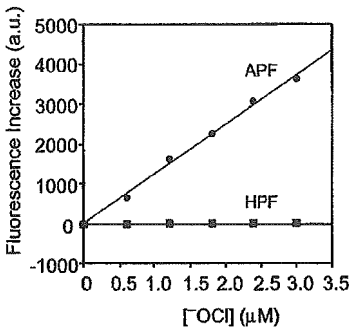

FIG. 3. **Detection of ⁻OCl by HPF and APF.** Relation between the concentrations of added NaOCl and fluorescence increase. HPF (*square*) or APF (*circle*) (final 10 μM; 0.1% DMF as a cosolvent) were added to sodium phosphate buffer (0.1 M, pH 7.4). The fluorescence intensity was determined at 515 nm with excitation at 490 nm.

TABLE I
Fluorescence increase of HPF, APF, and DCFH in various ROS generating systems

Dyes (final 10 μM, 0.1% DMF as a cosolvent) were added to sodium phosphate buffer (0.1 M, pH 7.4). The fluorescence intensities of HPF, APF, and DCFH were measured at 515, 515, and 520 nm with excitation at 490, 490, and 500 nm, respectively. DCFH was obtained by the hydrolysis of DCFH-DA with base as mentioned under "Experimental Procedures."

ROS	HPF	APF	DCFH
·OH[a]	730	1200	7400
$ONOO^-$[b]	120	560	6600
^-OCl[c]	6	3600	86
$^1O_2$[d]	5	9	26
O_2^-[e]	8	6	67
H_2O_2[f]	2	<1	190
NO[g]	6	<1	150
ROO·[h]	17	2	710
Autoxidation[i]	<1	<1	2000

[a] Ferrous perchlorate (100 μM) and H_2O_2 (1 mM) were added at room temperature.
[b] $ONOO^-$ (final 3 μM) was added at 37 °C.
[c] NaOCl (final 3 μM) was added at 37 °C.
[d] 3-(1,4-Dihydro-1,4-epidioxy-1-naphthyl)propionic acid (100 μM) was added and the mixtures were stirred at 37 °C for 30 min.
[e] KO_2 (100 μM) was added and the mixtures were stirred at 37 °C for 30 min.
[f] H_2O_2 (100 μM) was added and the mixtures were stirred at 37 °C for 30 min.
[g] 1-Hydroxy-2-oxo-3-(3-aminopropyl)-3-methyl-1-triazene (100 μM) was added and the mixtures were stirred at 37 °C for 30 min.
[h] 2,2′-Azobis(2-amidinopropane)dihydrochloride (100 μM) was added and the mixtures were stirred at 37 °C for 30 min.
[i] Dye solutions were placed under a fluorescent lamp for 2.5 h.

raphy and three-dimensional fluorescence spectroscopy (data not shown). Furthermore, we examined the relation between the concentration of ferrous perchlorate and the fluorescence increase in the Fenton reaction (Fig. 2*B*). Ferrous perchlorate was added at various concentrations to buffer solutions of HPF and APF containing an excess of H_2O_2. The results showed that the fluorescence increase is proportional to the concentration of ferrous perchlorate. Therefore, both HPF and APF can detect ·OH formed in the Fenton reaction in terms of a dose-dependent increase of fluorescence.

Reactivity of HPF and APF with ⁻OCl—^-OCl has a strong microbicidal activity, and plays a key role in the killing of bacteria by neutrophils (29, 30). Therefore, we investigated the reactivity of HPF and APF with ^-OCl. The results are shown in Fig. 3. Interestingly, the fluorescence intensity of APF greatly increased upon addition of ^-OCl, whereas that of HPF did not. In addition, the fluorescence increase of APF was dose-dependent. Therefore, we could detect ^-OCl selectively by using both HPF and APF together.

Reactivity of HPF, APF, and DCFH with Various ROS, and the Lability of the Probes to Light-induced Autoxidation—As mentioned above, DCFH is widely used as a fluorescence probe for ROS, but it lacks specificity among ROS and suffers from autoxidation; that is, the fluorescence increases even in the absence of ROS upon illumination. We compared the reactivities of HPF, APF, and DCFH with O_2^-, H_2O_2, ·OH, $^1O_2$, ^-OCl, NO, peroxynitrite ($ONOO^-$), and alkylperoxyl radical (ROO·). The observed fluorescence increases are shown in Table I. 3-(1,4-Dihydro-1,4-epidioxy-1-naphthyl)propionic acid thermally generates $^1O_2$ under mild conditions (31) and 1-hydroxy-2-oxo-3-(3-aminopropyl)-3-methyl-1-triazene thermally generates NO under mild conditions (32). 2,2′-Azobis(2-amidinopropane)dihydrochloride is an azo-initiator that forms alkyl radicals as a result of thermal decomposition, and these alkyl radicals can react with molecular oxygen to give alkylperoxyl radicals (33). Under these conditions, DCFH reacted unselectively with all of these reactive species. On the other hand, HPF and APF showed fluorescence augmentation only upon reaction with ·OH, $ONOO^-$, and/or ^-OCl, and not with O_2^-, H_2O_2, $^1O_2$, NO, ROO·, which are thought to be produced in many biological systems. $ONOO^-$ has a strong oxidizing power (34, 35), so it should be included in the category of hROS. Furthermore, DCFH was extensively autoxidized, resulting in a marked increase of the fluorescence intensity, whereas HPF and APF were not autoxidized at all. These results show that HPF and APF have much higher selectivity among ROS and a greater resistance to autoxidation than DCFH.

Next, we examined whether light-induced autoxidation would occur under conditions practically used for excitation in